





# Cation ATPase (ATP4) Orthologue Replacement in the Malaria Parasite *Plasmodium knowlesi* Reveals Species-Specific Responses to ATP4-Targeting Drugs

Franziska Mohring,<sup>a</sup> Donelly A. van Schalkwyk,<sup>a</sup> Ryan C. Henrici,<sup>b</sup> Benjamin Blasco,<sup>c\*</sup> Didier Leroy,<sup>c</sup>  Colin J. Sutherland,<sup>a,d</sup>  Robert W. Moon<sup>a</sup>

<sup>a</sup>Department of Infection Biology, Faculty of Infectious and Tropical Diseases, London School of Hygiene and Tropical Medicine, London, United Kingdom

<sup>b</sup>Center for Global Health, University of Pennsylvania School of Medicine, Philadelphia, Pennsylvania, USA

<sup>c</sup>Medicines for Malaria Venture, Geneva, Switzerland

<sup>d</sup>UK Health Security Agency Malaria Reference Laboratory, London School of Hygiene and Tropical Medicine, London, United Kingdom

Franziska Mohring and Donelly A. van Schalkwyk contributed equally to this work. Author order was determined alphabetically.

**ABSTRACT** Several unrelated classes of antimalarial compounds developed against *Plasmodium falciparum* target a parasite-specific P-type ATP-dependent Na<sup>+</sup> pump, PfATP4. We have previously shown that other malaria parasite species infecting humans are less susceptible to these compounds. Here, we generated a series of transgenic *Plasmodium knowlesi* orthologue replacement (OR) lines in which the endogenous *pkatp4* locus was replaced by a recodonized *P. knowlesi* *atp4* (*pkatp4*) coding region or the orthologous coding region from *P. falciparum*, *Plasmodium malariae*, *Plasmodium ovale* subsp. *curtisi*, or *Plasmodium vivax*. Each OR transgenic line displayed a similar growth pattern to the parental *P. knowlesi* line. We found significant orthologue-specific differences in parasite susceptibility to three chemically unrelated ATP4 inhibitors, but not to comparator drugs, among the *P. knowlesi* OR lines. The PfATP4<sup>OR</sup> transgenic line of *P. knowlesi* was significantly more susceptible than our control PkATP4<sup>OR</sup> line to three ATP4 inhibitors: cipargamin, PA21A092, and SJ733. The PvATP4<sup>OR</sup> and PmATP4<sup>OR</sup> lines were similarly susceptible to the control PkATP4<sup>OR</sup> line, but the PocATP4<sup>OR</sup> line was significantly less susceptible to all ATP4 inhibitors than the PkATP4<sup>OR</sup> line. Cipargamin-induced inhibition of Na<sup>+</sup> efflux was also significantly greater with the *P. falciparum* orthologue of ATP4. This confirms that species-specific susceptibility differences previously observed in *ex vivo* studies of human isolates are partly or wholly enshrined in the primary amino acid sequences of the respective ATP4 orthologues and highlights the need to monitor efficacy of investigational malaria drugs against multiple species. *P. knowlesi* is now established as an important *in vitro* model for studying drug susceptibility in non-falciparum malaria parasites.

**IMPORTANCE** Effective drugs are vital to minimize the illness and death caused by malaria. Development of new drugs becomes ever more urgent as drug resistance emerges. Among promising compounds now being developed to treat malaria are several unrelated molecules that each inhibit the same protein in the malaria parasite—ATP4. Here, we exploited the genetic tractability of *P. knowlesi* to replace its own ATP4 genes with orthologues from five human-infective species to understand the drug susceptibility differences among these parasites. We previously estimated the susceptibility to ATP4-targeting drugs of each species using clinical samples from malaria patients. These estimates closely matched those of the corresponding “hybrid” *P. knowlesi* parasites carrying introduced ATP4 genes. Thus, species-specific ATP4 inhibitor efficacy is directly determined by the sequence of the gene. Our novel approach to understanding cross-species susceptibility/resistance can strongly support the effort to develop antimalarials that effectively target all human malaria parasite species.

**Editor** Thomas E. Wellems, National Institute of Allergy and Infectious Diseases

**Copyright** © 2022 Mohring et al. This is an open-access article distributed under the terms of the [Creative Commons Attribution 4.0 International license](https://creativecommons.org/licenses/by/4.0/).

Address correspondence to Robert W. Moon, [Rob.Moon@lshtm.ac.uk](mailto:Rob.Moon@lshtm.ac.uk), or Donelly A. van Schalkwyk, [Don.vanSchalkwyk@lshtm.ac.uk](mailto:Don.vanSchalkwyk@lshtm.ac.uk).

\*Present address: Benjamin Blasco, Global Antibiotic Research and Development Partnership (GARDP), Geneva, Switzerland.

The authors declare a conflict of interest. B.B. was and D.L. is an employee of the funder, the Medicines for Malaria Venture. All other authors: no competing financial interests to declare.

**Received** 26 April 2022

**Accepted** 31 August 2022

**KEYWORDS** ATP4, CRISPR-Cas9, malaria, *Plasmodium falciparum*, *Plasmodium knowlesi*, *Plasmodium ovale*, *Plasmodium vivax*, antimalarial agents

Malaria continues to exert a substantial cost on human health, with 627,000 deaths from this disease estimated for 2020, despite encouraging progress toward elimination in some settings (1). *Plasmodium knowlesi*, a zoonotic malaria, accounted for almost all malaria cases reported in Malaysia in 2019 (3,212 *P. knowlesi* infections), with no indigenous cases of human malaria reported in that year (2). Importantly, *P. knowlesi* has been shown to exhibit a case fatality rate of 2.5/1,000 cases and is the most common cause of malaria deaths in Malaysia (3).

WHO guidelines recommend artemisinin combination therapy (ACT) for the treatment of uncomplicated malaria (4). Partial resistance to artemisinin derivatives and resistance to ACT partner drugs such as piperaquine has arisen in the Greater Mekong subregion (GMS) (5–7) and is now also being reported in Africa, where the burden of malaria is greatest (8, 9). If not checked, falling susceptibility to ACT in Africa would risk an increase in mortality, as was seen during the rise of chloroquine resistance in the late 20th century (10). New drug development is critical to circumvent this eventuality and maintain progress toward malaria elimination.

All drugs in use today for malaria treatment were identified before the turn of the century. However, with the development of high-throughput *in vitro* screens against live parasites, the last 2 decades have witnessed a revolution in malaria drug discovery, identifying numerous chemical scaffolds for drug development and several novel mechanisms of drug action (11–14). A particular success has been the development of the spiroindolone cipargamin (KAE609), which potently inhibits the growth of multi-drug-resistant *Plasmodium falciparum* lines *in vitro* and *Plasmodium vivax* and *P. falciparum* isolates *ex vivo*, with half-maximal effective concentration ( $EC_{50}$ ) values of <10 nM (15). Cipargamin was the first compound with a novel mechanism of action to enter human trials in 20 years (16). Spiroindolones, including cipargamin, disrupt  $Na^+$  homeostasis in malaria parasites, and spiroindolone-resistant lines harbor mutations in the gene encoding PfATP4, a *P. falciparum* P-type  $Na^+$  ATPase (17). Two unrelated antimalarial compounds, SJ733 and PA21A092, have also been shown to disrupt  $Na^+$  homeostasis in the malaria parasite, and mutations in PfATP4 are also implicated in resistance to these nonspiroindolone molecules (18, 19).

A collection of 525 structurally diverse compounds that target malaria parasites, assembled by the Medicines for Malaria Venture (MMV), has been made available to the scientific community for evaluation. Thirty-nine of these structurally diverse antimalarial chemotypes have been shown to disrupt  $Na^+$  homeostasis in the malaria parasite (20, 21). This convergence around a single cellular process (regulation of intracellular sodium concentration through ATP4) confirms this as a critical drug target and a potential Achilles heel for the parasite.

ATP4 is an essential protein (22) that is localized to the parasite plasma membrane (15). Inhibition of ATP4 causes an increase in the parasite's intracellular  $Na^+$  concentration ( $[Na^+]_i$ ) and a concomitant increase in cytosolic pH (17). While ATP4 was initially annotated as a  $Ca^{2+}$  transporter (23), current evidence supports ATP4 functioning as a  $Na^+$  efflux ATPase that exports  $Na^+$  while importing  $H^+$  (17).

While multiple ATP4 inhibitors have been identified as highly potent against *P. falciparum* *in vitro* and *ex vivo*, evidence of potency against other malaria species has been mixed. Cipargamin and the pyrazoleamide PA21A092 were shown to be effective against both *P. falciparum* and *P. vivax* parasites using *ex vivo* screens (15, 19), although  $EC_{50}$  data generated in this way is difficult to compare cross-species due to the large variance in the estimates for *P. vivax*. However, the dihydroisoquinolone SJ733 was estimated to be 10-fold less potent against *Plasmodium berghei* and two other murine malaria species than against *P. falciparum* using *ex vivo* tests (18). We have previously compared the activities of ATP4 inhibitors against *P. falciparum* (3D7 clone) and the zoonotic *P. knowlesi* (A1-H.1 clone) under identical *in vitro* conditions. *P. knowlesi* was found to be approximately 6-fold less susceptible to cipargamin, SJ733, and PA21A092 than *P. falciparum* (24). Furthermore, we confirmed that

two other human-infecting malaria parasites (*Plasmodium malariae* and *Plasmodium ovale* spp.) are 5- to 7-fold less susceptible to cipargamin than *P. falciparum* when tested under identical *ex vivo* conditions (25). This suggests that there may be important species differences in susceptibility to these ATP4 inhibitors, with *P. falciparum* being the most susceptible of the human malaria species so far tested.

In an effort to explain the differences in susceptibility of SJ733 between the murine malaria species and *P. falciparum*, Jimenez-Diaz et al. performed an ATP4 orthologue replacement (ATP4<sup>OR</sup>) in *P. berghei* (18). The authors found that when the *P. berghei* *atp4* (*pbatp4*) gene was replaced with *pfatp4*, the resulting parasites were more susceptible to SJ733 in their *ex vivo* screen (18). This suggests sequence variation between the *pbatp4* and *pfatp4* genes is responsible for the species differences in susceptibility to SJ733. It remains unknown whether the differences we have observed in susceptibility to multiple ATP4 inhibitors among the human-infecting malaria species are similarly determined by sequence variations among the different orthologue genes.

To further understand and characterize observed differences in susceptibility to ATP4 inhibitors among human-infecting malaria species, we applied an orthologue replacement (OR) approach in our now well-established *P. knowlesi* *in vitro* drug susceptibility model. We replaced the endogenous *pkatp4* gene with codon-harmonized *atp4* genes from each of the other human-infecting malaria species: *P. falciparum* (*pfatp4*), *P. vivax* (*pvatp4*), *P. malariae* (*pmatp4*), *P. ovale* subsp. *curtisi* (*pocatp4*), and *P. knowlesi* (*pkatp4*). We then compared the *P. knowlesi* transfectant lines to assess growth rates, drug susceptibility, and potential changes in [Na<sup>+</sup>]<sub>i</sub> and pH. Finally, we used molecular modeling to explore potential mechanistic explanations for the species differences identified among our transfectant lines.

## RESULTS

**Orthologue replacement of ATP4 in *P. knowlesi* does not impact parasite growth.** We utilized our *in vitro* *P. knowlesi* model to study possible species differences in susceptibility to ATP4 inhibitors. We have previously shown the value of adapting our *P. knowlesi* model to evaluate *P. vivax* Duffy binding protein vaccine candidates (26, 27). As with *P. malariae* and *P. ovale* spp., *P. vivax* lacks a long-term *in vitro* culture system (28).

Transgenic *P. knowlesi* A1-H.1 parasites were generated using the CRISPR-Cas9 genome editing approach described by Mohring et al. (26). The entire locus of *pkatp4* was replaced with either a recodonomized version (PkATP4<sup>OR</sup>), which encodes an identical amino acid sequence with altered codon usage at the nucleotide level, or recodonomized ATP4 orthologues of *P. vivax*, *P. falciparum*, *P. malariae*, and *P. ovale* subsp. *curtisi* (PlasmoDB.org) (29–33) (Fig. 1A). Following cotransfection of each plasmid bearing a synthetic ATP4 orthologue together with the Cas9-containing companion plasmid, successful integration was readily achieved for all ATP4 orthologues and clonal lines established for each by limiting dilution cloning (Fig. 1B). ATP4 is essential for malaria parasite survival (22); thus, the successful replacement of *pkatp4* indicates that the *P. falciparum*, *P. vivax*, *P. malariae*, and *P. ovale* subsp. *curtisi* orthologues can complement its cellular function. Furthermore, growth assays showed no significant differences between the parental *P. knowlesi* A1-H.1 line and the five transgenic lines (Fig. 1C).

**ATP4 orthologue replacement in *P. knowlesi* confers species differences in susceptibility to ATP4 inhibitors but not to comparator drugs.** To investigate the susceptibility of the different *Plasmodium* ATP4 orthologues to ATP4 inhibitors in the heterologous *P. knowlesi* cell, we conducted *in vitro* growth inhibition assays. Parasite lines, set to the same starting parasitemia and hematocrit, were exposed to serial dilutions of cipargamin, PA21A092, and SJ733 for one complete parasite life cycle (27 h). We also exposed each orthologue replacement line (denoted here by the superscript “OR”) to chloroquine and dihydroartemisinin, which exert their antimalarial effects independently of ATP4, as comparators. As expected, we did not observe significant differences in chloroquine or dihydroartemisinin susceptibility among the parental and orthologue replacement lines, nor were parental *P. knowlesi* parasites different in susceptibility to these drugs than the PkATP4<sup>OR</sup>

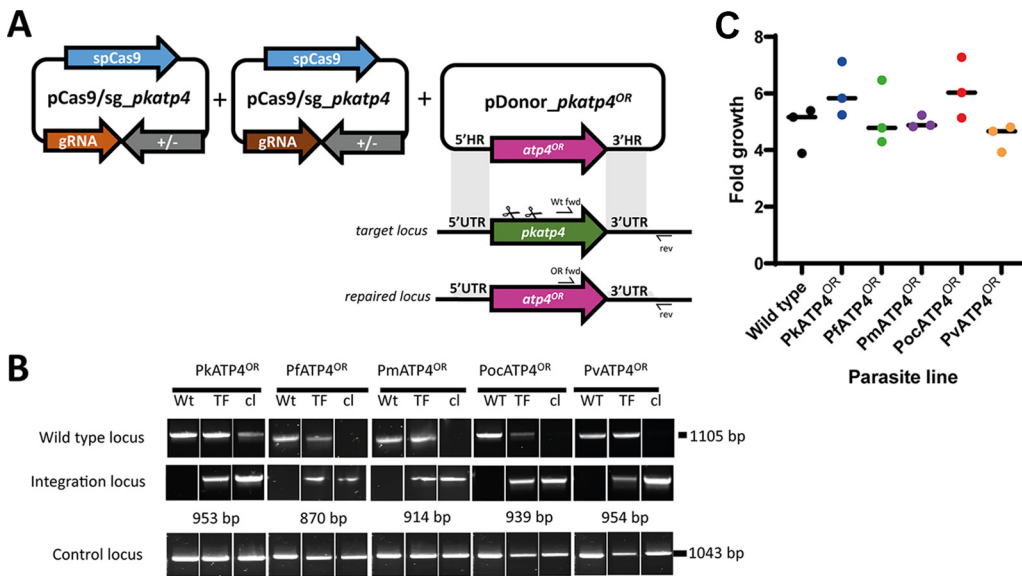


**FIG 1** Orthologue replacement (OR) of *Plasmodium knowlesi* ATP4. (A) Schematic of CRISPR-Cas9 genome editing strategy. Integration of *atp4* orthologues into the target *pkatp4* locus was via homologous recombination. Arrows indicate oligonucleotide positions for diagnostic PCRs. (B) Parasites transfected (TF) with pCas9/sg\_ATP4 and pDonor\_orthologue plasmids were analyzed with diagnostic PCRs. Shown are results from PCRs detecting the wild-type locus (i.e., from the parental A1-H.1 clone) (Wt fwd + rev) and integration locus (Int fwd + rev) as well as a control PCR targeting an unrelated locus (PKMTIP fwd + PKMTIP rev). The WT locus band for the PkATP4<sup>OR</sup> clonal line was confirmed as PkATP4<sup>OR</sup> by amplicon sequencing. (C) Graph showing fold multiplication of WT, PkATP4<sup>OR</sup>, PfATP4<sup>OR</sup>, PmATP4<sup>OR</sup>, PocATP4<sup>OR</sup>, or PvATP4<sup>OR</sup> parasites in erythrocytes over one intraerythrocytic growth cycle (27 h). Assays were carried out in technical duplicates in Duffy-positive erythrocytes with three independent biological replicates. A one-way ANOVA revealed there was no statistically significant difference in growth rates between at least two groups:  $F(5, 12) = [1.966]$  and  $P = 0.16$ .

line, suggesting that the orthologue replacement process itself had not caused a general perturbation of drug responses (Fig. 2 and Table 1).

Among the ATP4 inhibitors screened, cipargamin was the most potent against all parasite lines, followed by PA21A092, while SJ733 was the least potent (Table 1). The PfATP4<sup>OR</sup> transgenic line was the most susceptible to all ATP4 inhibitors tested (Fig. 2 and Table 1). For all ATP4 inhibitors, the PfATP4<sup>OR</sup> line was significantly more susceptible than the control PkATP4<sup>OR</sup> line (7- to 8-fold change) (see Table S1 in the supplemental material), which was in turn similar in susceptibility to PvATP4<sup>OR</sup> and PmATP4<sup>OR</sup> (Fig. 2, Table 1, and Table S1). Conversely, the PocATP4<sup>OR</sup> line was significantly less susceptible to all ATP4 inhibitors than the control PkATP4 line ( $P < 0.0001$ ) (Table 1 and Fig. 2). Notably, the PocATP4<sup>OR</sup> line exhibited EC<sub>50</sub> values 21, 33.7, and 14.9 times higher than those for the PfATP4<sup>OR</sup> line for cipargamin, PA21A092, and SJ733, respectively (Table S1).

For comparison, we include also previous data that we published for our *P. knowlesi* A1-H.1 line and *P. falciparum* 3D7 line in Table 1 (24, 34). As expected, the *P. knowlesi* EC<sub>50</sub> estimates reported by us previously are similar to those derived here for the parental *P. knowlesi* line, this being the same parasite line (Table 1). Importantly, the susceptibility of the PfATP4<sup>OR</sup> line to the three ATP4 inhibitors is similar to the susceptibility of the *P. falciparum* 3D7 line (24). However, the PfATP4<sup>OR</sup> line is not similar in susceptibility to chloroquine or dihydroartemisinin compared to the *P. falciparum* line (Table 1). For these two comparator drugs, the susceptibility phenotype of the PfATP4<sup>OR</sup> line is similar to that of the parental *P. knowlesi* line.

**Effect of orthologue replacement on intracellular sodium ([Na<sup>+</sup>]<sub>i</sub>).** Previous research by Spillman et al. used the sodium-sensitive fluorescent dye SBFI to measure the resting intracellular sodium concentration ([Na<sup>+</sup>]<sub>i</sub>) of *P. falciparum* 3D7 parasites and the impact of adding ATP4 inhibitors on the resting [Na<sup>+</sup>]<sub>i</sub> (17). They demonstrated that *P. falciparum* maintains a resting [Na<sup>+</sup>]<sub>i</sub> of around 11 mM, and the addition of ATP4 inhibitors caused a dose-dependent increase in [Na<sup>+</sup>]<sub>i</sub> (17). We observe average

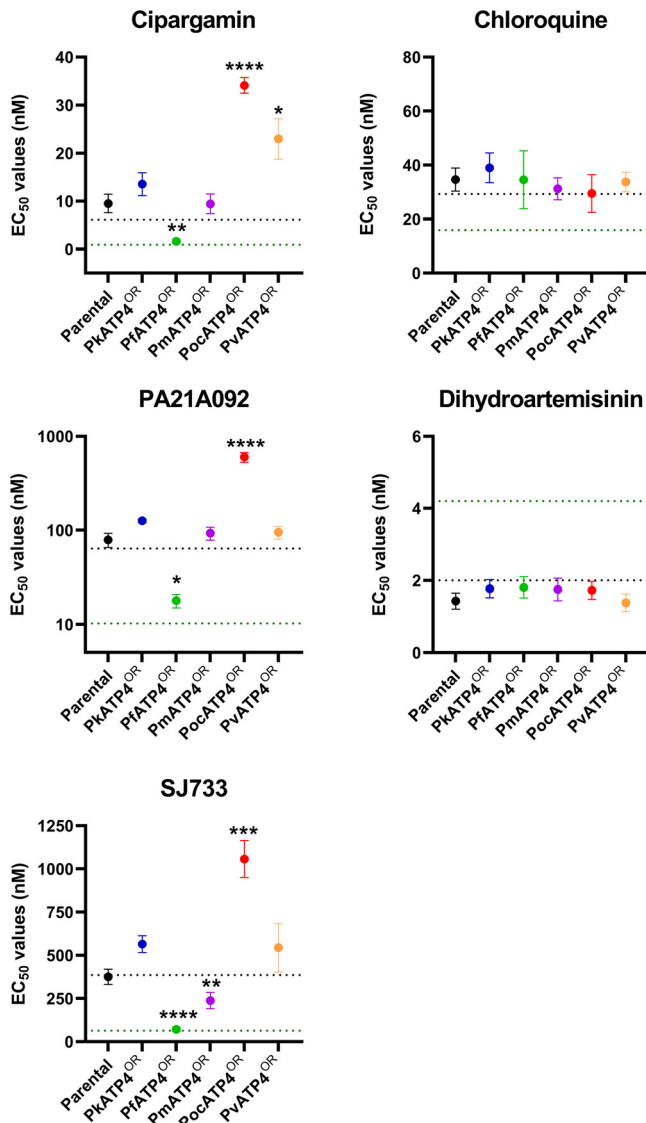


**FIG 2** Drug susceptibility of orthologue replacement lines. Parental or orthologue replacement (OR) lines were exposed to serial dilutions of ATP4 inhibitors (cipargamin, PA21A092, and SJ733) or control drugs (chloroquine and dihydroartemisinin) for one complete parasite life cycle (27 h). Parasite viability was measured using the SYBR green I fluorescence method. Data show the mean EC<sub>50</sub> values (nanomolar concentration) from at least three experiments, with some including up to eight repeats. Error bars represent the standard error of the mean (SEM). Stars indicate parasite lines that were significantly different ( $P < 0.05$ ) from the PkATP4<sup>OR</sup> line (blue circles). For comparison also, using dotted lines, we plot where our previously published drug susceptibility data lie for the PkA1.H-1 (black lines) and Pf3D7 (green lines) parasite lines. These published data (24, 34) were from experiments performed under conditions identical (i.e., one life cycle exposure) to those used in the current study on the orthologue replacement lines. Note that the graph for PA21A092 is plotted using a log scale for clarity. All other graphs plot linear scales. \*,  $P \leq 0.05$ ; \*\*,  $P \leq 0.01$ ; \*\*\*,  $P \leq 0.001$ ; \*\*\*\*,  $P \leq 0.0001$ .

resting  $[Na^+]_i$  values for our orthologue replacement lines of between 12.7 mM (PfATP4<sup>OR</sup> line) to 22.0 mM (PocATP4<sup>OR</sup> line) (Fig. 3A and Table 2). These resting  $[Na^+]_i$  values of the transgenic lines were all slightly higher than the parental *P. knowlesi* line (8.75 mM) and the *P. falciparum* 3D7 line (6.34 mM) (Fig. 3), but these differences were not statistically significant compared to the PkATP4<sup>OR</sup> line ( $P \geq 0.0765$ ) (Table 2).

Upon addition of the ATP4 inhibitor cipargamin, we observed a dose-dependent increase in the  $[Na^+]_i$  for all the parasite lines tested (a representative curve is shown in Fig. 3B), with improved signal-to-noise ratios at the higher drug concentration of 100 nM. To distinguish between the responses of different orthologue replacement lines, we calculated and



**TABLE 1** Drug susceptibility of the parental *P. knowlesi* (A1-H.1 clone) and orthologue replacement lines to ATP4 inhibitors (cipargamin, PA21A092, and SJ733) and control drugs (chloroquine and dihydroartemisinin)<sup>a</sup>

Parasite line	EC <sub>50</sub> , nM (P value)				
	Cipargamin	PA21A092	SJ733	Chloroquine	Dihydroartemisinin
Parental	9.51 ± 1.9 (0.5878)	78.8 ± 13.6 (0.7185)	375 ± 44 (0.2104)	34.6 ± 4.3 (0.9899)	1.43 ± 0.22 (0.9238)
PkATP4 <sup>ORb</sup>	13.5 ± 2.4 (NA) <sup>b</sup>	126 ± 5.5 (NA)	565 ± 48 (NA)	39.0 ± 5.5 (NA)	1.77 ± 0.25 (NA)
PfATP4 <sup>OR</sup>	1.62 ± 0.37 (0.0019)	17.8 ± 2.9 (0.0317)	71 ± 11 (<0.0001)	34.6 ± 10.8 (0.9924)	1.81 ± 0.29 (0.9999)
PmATP4 <sup>OR</sup>	9.44 ± 2.0 (0.5698)	92.8 ± 14.7 (0.9072)	238 ± 47 (0.0069)	31.2 ± 4.1 (0.8382)	1.75 ± 0.31 (0.9999)
PocATP4 <sup>OR</sup>	34.1 ± 1.6 (<0.0001)	599 ± 70 (<0.0001)	1057 ± 107 (0.0001)	29.5 ± 7.0 (0.8222)	1.73 ± 0.25 (0.9999)
PvATP4 <sup>OR</sup>	22.9 ± 4.2 (0.0172)	94.8 ± 14.6 (0.9433)	544 ± 140 (0.9997)	33.7 ± 3.6 (0.9845)	1.39 ± 0.24 (0.8725)
PkA1-H1 <sup>c</sup>	6.1 ± 0.5 (0.0647)	63.8 ± 7.6 (0.3618)	386 ± 34 (0.2222)	29.3 ± 4.7 (0.6665)	2.03 ± 0.25 (0.9824)
PF3D7 <sup>c</sup>	0.89 ± 0.08 (0.0006)	10.2 ± 1.4 (0.0139)	64.3 ± 4.3 (<0.0001)	15.9 ± 3.0 (0.0222)	4.16 ± 0.52 (<0.0001)

<sup>a</sup>Parasites were exposed to drugs for one complete *in vitro* life cycle (27 h), and viability was measured using the SYBR green I method. Drug assays were run in technical duplicates on at least three biological replicates (up to eight times). Values are the mean ± SEM. P values were determined from *post hoc* analysis comparing EC<sub>50</sub> data from all species to PkATP4<sup>OR</sup> data using Dunnett's test.

<sup>b</sup>NA, not applicable (as this is the comparator line).

<sup>c</sup>Data published previously on the *P. knowlesi* A1-H.1 line and on the *P. falciparum* 3D7 line in references 24 and 34 tested under identical conditions to the other lines tested here.

compared the rates of increase in [Na<sup>+</sup>]<sub>i</sub> from steady state for 10 min following the addition of 100 nM cipargamin to the parasites, as well as the maximum increase in [Na<sup>+</sup>]<sub>i</sub> over that time. This period of time was selected as previous data showed Na<sup>+</sup> accumulation continuing to increase linearly at 10 min until the curve begins to flatten after 60 min (18). This linear increase 10 min after drug exposure was observed also for all the lines tested in our assays. When we compared the rates of increase in the [Na<sup>+</sup>]<sub>i</sub> after 10 min of cipargamin exposure, we observed a significant difference only between the PfATP4<sup>OR</sup> line compared to the control PkATP4<sup>OR</sup> line ( $P = 0.0002$ ) (Table 2 and Fig. 3C). The rate of [Na<sup>+</sup>]<sub>i</sub> increase for the PfATP4<sup>OR</sup> line (203.2 μM/s) was over 5 times faster than that for the PkATP4<sup>OR</sup> line (35.8 μM/s) (Table 2) in the first 10 min after exposure to the inhibitor. None of the other lines were significantly different from the PkATP4<sup>OR</sup> line with respect to their rate of [Na<sup>+</sup>]<sub>i</sub> increase within the first 10 min after cipargamin exposure ( $P \geq 0.2618$ ) (Table 2 and Fig. 3C). When comparing the magnitudes of the increase in [Na<sup>+</sup>]<sub>i</sub> among the parental and orthologue replacement lines over the 10-min exposure to cipargamin, we observed increases from steady state of between 18 and 35 mM for most lines, and these values were not significantly different from those of the PkATP4<sup>OR</sup> line ( $P \geq 0.9972$ ) (Table 2). However, exposure to 100 nM cipargamin in the PfATP4<sup>OR</sup> line for 10 min produced a maximum increase in [Na<sup>+</sup>]<sub>i</sub> of 138.6 mM (Table 2), significantly higher than that in the PkATP4<sup>OR</sup> line ( $P = 0.0007$ ) (Table 2). The PvATP4<sup>OR</sup> line experienced an intermediate maximum increase in [Na<sup>+</sup>]<sub>i</sub> of 81.1 mM after cipargamin exposure, but this value was not significantly different from that of the PkATP4<sup>OR</sup> reference line ( $P = 0.1312$ ) (Table 2). Thus, the magnitude of this rapid, cipargamin-induced inhibition of Na<sup>+</sup> efflux was lower for all non-falciparum orthologue replacement lines than those of the PfATP4<sup>OR</sup> line and suggests that intracellular drug has an immediate impact on ATP4 function in *P. knowlesi*, but this is much more profound for the *P. falciparum* ATP4 than for its orthologues from other human-infecting members of the genus.

**Effect of orthologue replacement on pH<sub>i</sub> (pH<sub>cyt</sub>).** *P. falciparum* maintains a resting cytosolic pH (pH<sub>cyt</sub>) of around 7.3 through its plasma membrane-localized V-type H<sup>+</sup>-ATPase (35). Inhibition of this V-type H<sup>+</sup>-ATPase by the inhibitor bafilomycin A<sub>1</sub> (35) or concanamycin A (36) induces a rapid acidification within the parasite cytosol. Using the pH-sensitive fluorophore BCECF [2',7'-bis-(2-carboxyethyl)-5-(and-6)-carboxyfluorescein], we demonstrate that parental and transfectant *P. knowlesi* lines maintain a similar resting pH to that of *P. falciparum*, between 7.24 and 7.28 (Table S2). We show also that, in *P. knowlesi*, the addition of concanamycin A (100 nM) causes a rapid acidification of the cytosolic pH (Fig. 4A), similar to that observed for *P. falciparum* previously.

In contrast to inhibitors of the V-type H<sup>+</sup>-ATPase, which acidify of the cytosol, inhibitors of ATP4, a P-type ATPase, have been shown to rapidly alkalize the cytosol in *P. falciparum* (17, 18). We demonstrate here that, in *P. knowlesi*, addition of cipargamin

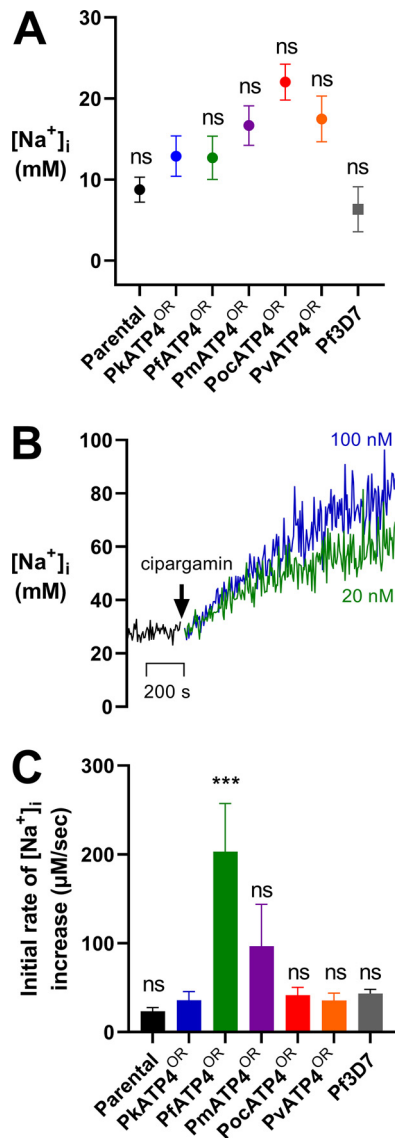


**FIG 3** Resting intracellular sodium concentration ( $[Na^+]_i$ ) of the orthologue replacement lines and the concentration-dependent increase in  $[Na^+]_i$  after addition of cipargamin. Trophozoite-stage parasites were loaded with the  $Na^+$ -sensitive fluorophore SBF1, and the fluorescence of the suspensions was measured in a spectrophotometer. (A) Measurements of resting  $[Na^+]_i$  show values of between 6.34 mM for the *P. falciparum* 3D7 line (gray square) and 22.03 mM for the PocATP4<sup>OR</sup> line (red circle). However, there was no significant difference for any of the lines compared to the PfATP4<sup>OR</sup> line (green circle;  $P > 0.0681$ ). Data show the mean  $\pm$  SEM. (B) Addition of cipargamin resulted in an immediate dose-dependent increase in the resting  $[Na^+]_i$  inside all parasite lines. Shown here are representative traces from a single experiment demonstrating the impact of adding 20 nM cipargamin (green trace) or 100 nM cipargamin (blue trace) on the resting  $[Na^+]_i$  of the PocATP4<sup>OR</sup> line. (C) Addition of 100 nM cipargamin to the parasite lines results in an increase in the  $[Na^+]_i$  from steady state. We determined the initial rate of increase in the  $[Na^+]_i$  by fitting a linear regression curve to the  $[Na^+]_i$  increase data across that 10-min exposure. The slope of that curve provides the rate of increase (in micromolar concentration per second). Experiments for resting  $[Na^+]_i$  were performed in technical duplicates for at least three biological repeats, but some were performed to eight times. Experiments for the initial rate of increase in  $[Na^+]_i$  were performed in technical duplicates for at least three biological repeats, but some were performed up to five times. \*\*\*,  $P \leq 0.001$ ; ns, non significant ( $P > 0.05$ ).

causes a dose-dependent increase in the cytosolic pH (Fig. 4B). In our experiments on the *P. falciparum* 3D7 line, we report an intracellular pH (pH<sub>i</sub>) of  $7.45 \pm 0.04$ , which was significantly different from that of the *P. knowlesi* PkATP4<sup>OR</sup> line ( $P = 0.0291$ ) (Table S2), suggesting resting pH is dependent on multifactorial differences in pH homeostasis control between the two parasite species and not governed by ATP4 specifically, as

**TABLE 2** Comparison of the resting intracellular sodium concentration ( $[Na^+]_i$ ) and the rate of increase and maximum increase in the  $[Na^+]_i$  after a 10-min exposure to 100 nM cipargamin in the *P. knowlesi* A1-H.1 parental and orthologue replacement lines and the *P. falciparum* 3D7 line<sup>a</sup>

Parasite line	Resting $[Na^+]_i$ , mM ( <i>P</i> value)	Rate of increase in $[Na^+]_i$ 10 min after cipargamin exposure, $\mu$ M/s ( <i>P</i> value)	Maximum increase in $[Na^+]_i$ 10 min after cipargamin exposure, mM ( <i>P</i> value)
Parental	8.75 $\pm$ 1.54 (0.7587)	23.3 $\pm$ 4.26 (0.9952)	17.9 $\pm$ 3.23 (0.9974)
PkATP4 <sup>ORb</sup>	12.9 $\pm$ 2.48 (NA) <sup>b</sup>	35.8 $\pm$ 9.98 (NA)	26.2 $\pm$ 8.08 (NA)
PfATP4 <sup>OR</sup>	12.7 $\pm$ 2.67 (>0.9999)	203.2 $\pm$ 54.1 (0.0002)	138.6 $\pm$ 34.1 (0.0007)
PmATP4 <sup>OR</sup>	16.7 $\pm$ 2.43 (0.8913)	35.7 $\pm$ 8.07 (0.9999)	27.5 $\pm$ 6.59 (0.9999)
PocATP4 <sup>OR</sup>	22.0 $\pm$ 2.21 (0.0765)	41.5 $\pm$ 8.85 (0.9997)	35.4 $\pm$ 7.97 (0.9962)
PvATP4 <sup>OR</sup>	17.5 $\pm$ 2.81 (0.5835)	96.6 $\pm$ 47.3 (0.2618)	81.1 $\pm$ 39.9 (0.1312)
Pf3D7	6.34 $\pm$ 2.78 (0.3963)	43.5 $\pm$ 4.84 (0.9996)	33.3 $\pm$ 4.41 (0.9978)

<sup>a</sup>Resting  $[Na^+]_i$ , rate of increase, and maximum increase data were measured in SBFI-loaded saponin-isolated late-stage trophozoites suspended in physiological saline. All data show the mean  $\pm$  SEM. Experiments for resting  $[Na^+]_i$  were performed in duplicate on at least three occasions, but some were performed up to eight times.

Experiments for rate of increase in  $[Na^+]_i$  and maximum increase in  $[Na^+]_i$  were performed in technical duplicates performed on at least three biological repeats (up to five times). *P* values were calculated using ANOVA with Dunnett's multiple-comparison test comparing the lines to the PkATP4<sup>OR</sup> line.

<sup>b</sup>NA, not applicable (as this is the comparator line).

expected (35, 37). The orthologue replacement lines all displayed a resting  $pH_i$  similar to that of the parental *P. knowlesi* line (Fig. 4C).

In each line, a 10-min exposure to 100 nM cipargamin caused a small change compared to resting  $pH_i$  (Fig. 4D and Table S2). For the parental *P. knowlesi* line this was a 0.4%  $\pm$  0.1% increase in  $pH_i$  (Table S2), and it was almost identical to that shown by the orthologue replacement lines PkATP4<sup>OR</sup> (0.6%  $\pm$  0.04% increase) and PfATP4<sup>OR</sup> (0.6%  $\pm$  0.07% increase). The PocATP4<sup>OR</sup> and PvATP4<sup>OR</sup> lines were also tested and gave similar, small increases in  $pH_i$  (0.5%  $\pm$  0.01% and 0.4%  $\pm$  0.01%).

**Molecular modeling.** Alignment of each of the ATP4 orthologues from *P. berghei* and the human-infective species demonstrates that the differences in susceptibility do not appear to correlate with previous markers of PfATP4 resistance (Fig. S1). Indeed, three PfATP4 resistance-conferring residues identified through selection of *P. falciparum* with ATP4 inhibitors are conserved in the wild-type (WT) *atp4* gene sequence of all orthologues (18). Differences in orthologue susceptibility are thus likely to result from distinct mechanisms from those observed for *in vitro*-selected resistance. Previous work in *P. berghei* has also suggested that a 5-amino-acid loop of primary sequence diversity could also account for differences in species susceptibility (Fig. 5 and Fig. S1) (18). However, this sequence is more conserved among the human-infective species, particularly *P. ovale*, which harbors a single nonidentical amino acid and single similar amino acid within the loop.

In order to investigate structural differences among the protein orthologues that could explain our observations of phenotypic differences in ATP4 inhibitor susceptibility, we performed molecular modeling and docking experiments *in silico*. Models for PfATP4 were generated *de novo* using the Iterative Threading Assembler (I-TASSER) as described and compared with the primary model described by Jimenez-Diaz et al. (18), with good alignment noted (root mean square deviation [RMSD] of 2.4 Å over all atoms). Subsequently, threading models were built for the other ATP4 homologs based on this template, and structure-sequence similarity was compared by alignment (Fig. 5, upper panel). Overlay of the model ATP4 homolog structures revealed high similarity between the core transmembrane (TM) domains, with most structural dissimilarity occurring in the extracellular domain. Consistently, most sequence diversity, with respect to *Plasmodium* versus *Plasmodium* and *Plasmodium* versus non-*Plasmodium* ATP4 orthologues, also occurs in this extracellular domain (Fig. 5, upper panel; Clustal alignment in Fig. S1).

Next, we docked the structures of (+)-SJ733 and cipargamin to each homolog using AutoDock, where the drug molecules were permitted to flex and rotate as chemistry and steric restrictions allowed. We reidentified the putative solvent-exposed drug-binding pocket noted by Jimenez-Diaz et al. (18), further supporting the validity of our



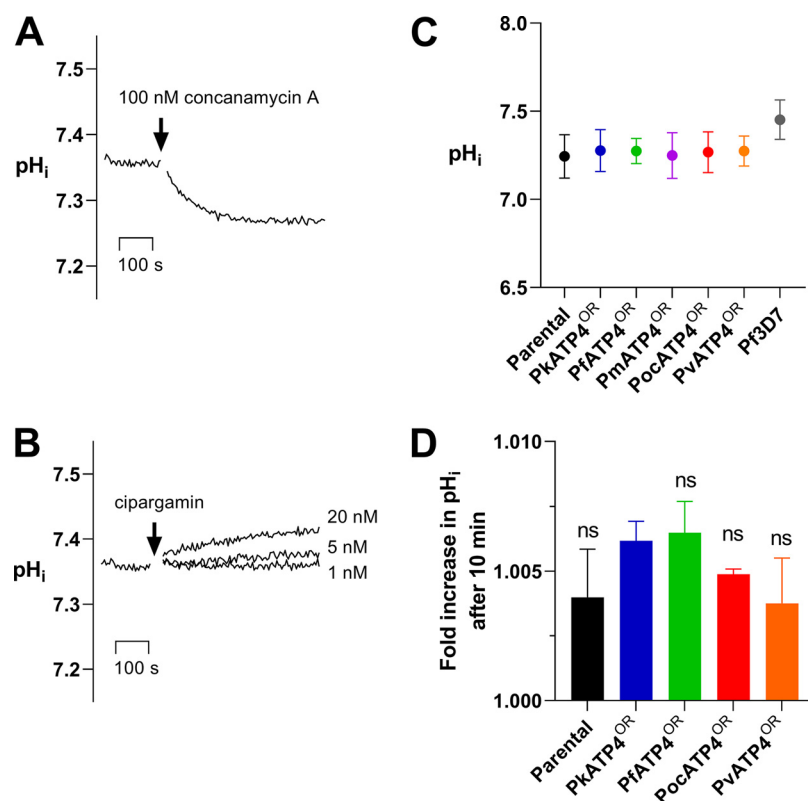


**FIG 4** Resting cytosolic pH of orthologue replacement lines and the concentration-dependent increase in pH after addition of cipargamin. Trophozoite-stage parasites were loaded with the pH-sensitive fluorophore BCECF, and the fluorescence of the suspensions was measured in a spectrophotometer. (A) Addition of 100 nM concanamycin A, a V-type  $H^+$ -ATPase inhibitor, caused a rapid acidification of the  $pH_i$  for the *P. knowlesi* parental line as shown before in *P. falciparum* (35). Shown here is a trace from a single experiment, but it is representative of results obtained on multiple occasions and in all lines. (B) Dose-dependent effect of adding the ATP4 inhibitor cipargamin on alkalinization of  $pH_i$  in the *P. knowlesi* parental line. Data shown are the average from at least 3 independent biological replicates  $\pm$  SEM (C) Measurements of baseline  $pH_i$  show no significant difference among the *P. knowlesi* parental parasites and the orthologue replacement lines ( $pH_i \sim 7.25$ ). The *P. falciparum* intracellular pH was slightly higher (7.45). (D) We determined the fold increase in  $pH_i$  after the addition of 100 nM cipargamin to the parasite lines. The fold increase was determined by dividing the  $pH_i$  at 10 min by the resting  $pH_i$  before the addition of cipargamin ( $t = 0$  min). Data for the resting pH experiments are from technical duplicate experiments performed with at least five biological repeats (up to 10 times). Data from the fold change in pH experiments are from duplicate experiments performed on two to three separate occasions. ns, non significant ( $P > 0.05$ ).

models. Interestingly, the docking solutions for each homolog are structurally different, with the drug molecules rotating or lifting within the pockets to optimize stabilizing interactions (Fig. 6). This is likely due to slight differences in the diameter of the binding pocket based on the positions of the large transmembrane helices, which may or may not be artifactual to the modeling process. We calculated and compared the dissipated free energy of the top docking solution for cipargamin and SJ733 for each orthologue (Fig. 6). While PocATP4-cipargamin did exhibit a  $|\Delta\Delta G|$  of 1.3 kcal/mol with respect to PfATP4-cipargamin, predicting a significant lower stability of binding that may contribute to lower susceptibility of PocATP4<sup>OR</sup> to cipargamin *in vitro*, there was no relationship between orthologues rank ordered by  $\Delta\Delta G$  (versus PfATP4) or fold difference in  $EC_{50}$  (versus PfATP4<sup>OR</sup>) for either compound. We note the short, 5-amino-acid loop of primary sequence diversity noted by Jimenez-Diaz that is structurally located near the drug-binding pocket (Fig. 5, upper right corner of inset, and Fig. S1). In all of the homology models, this loop does not have predicted secondary structure and occupies approximately the same spatial location, more than 20 Å away from the nearest atom of (+)-SJ733 or cipargamin. Furthermore, the helices located immediately downstream of this loop that are predicted to contact the drug molecules align well,

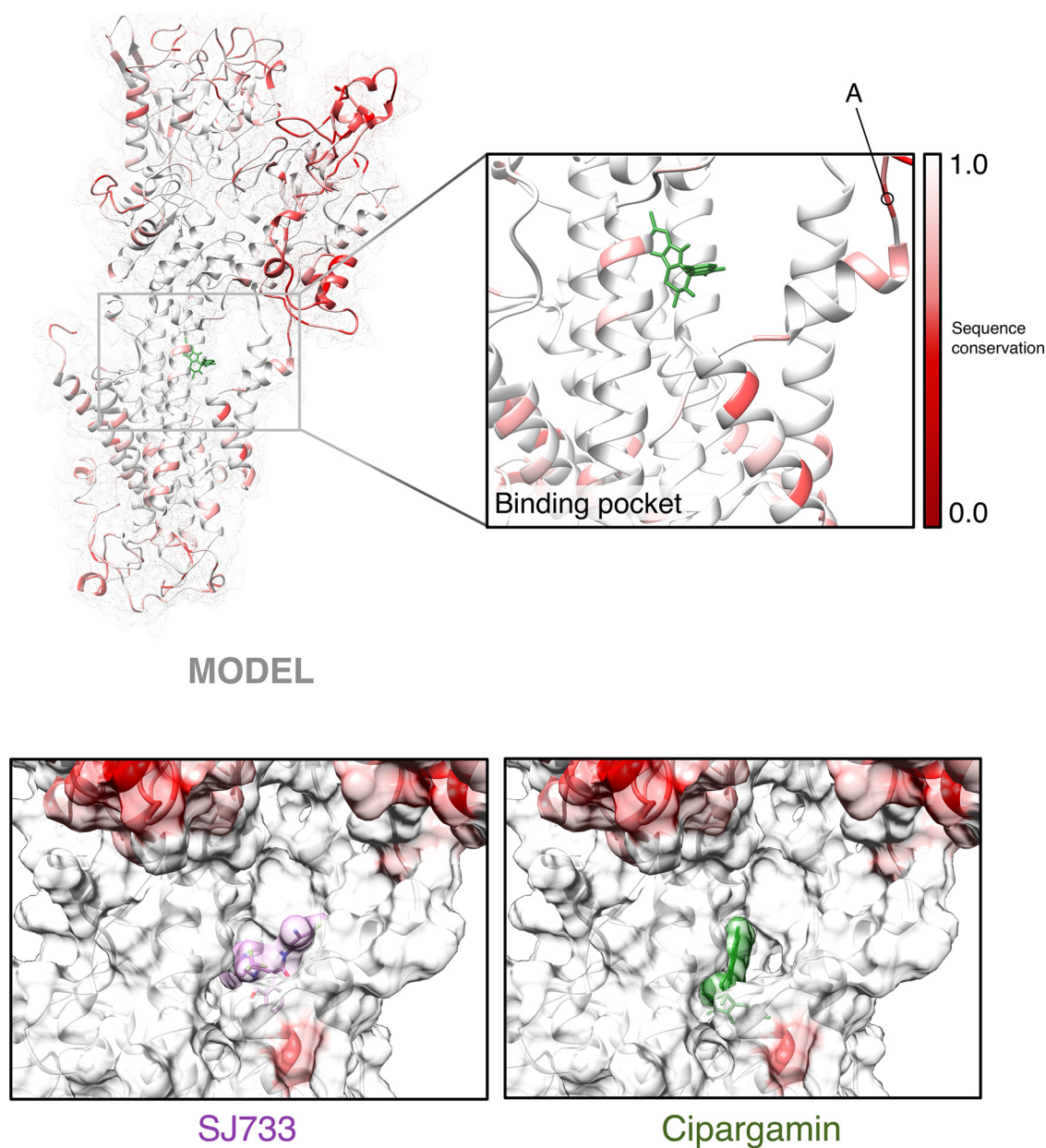


**FIG 5** Molecular models of ATP4 orthologues and reidentification of the solvent-exposed spiroindolone drug-binding pocket. (Top panel) Structural model of PfATP4 colored by sequence conservation as determined by multiple-sequence alignment of *Plasmodium* ATP4 orthologues described in this study. Red indicates no sequence identity, whereas white indicates perfect conservation across all orthologues on a per-amino-acid basis. The inset shows the drug-binding pocket identified by docking drug molecules across the entire solvent-exposed protein surface. “A” indicates the 5-amino-acid peptide identified by Jimenez-Diaz et al. (18) as associated with SJ733 susceptibility. (Bottom panels) Surface maps with false coloring as described above showing SJ733 and cipargamin docked within the identified drug-binding pocket in the context of our PfATP4 model.

suggesting no gross deformations in the drug pocket because of this diversity. While we cannot rule out that this loop may displace structures required for drug binding, our docking simulations did not identify any significant structural effects contributed by this loop.

We also compared our PfATP4 homology model to the DeepMind AlphaFold (AF)-predicted PfATP4 model (38), PfATP4\_AF(120–1263), and noted that most of the structural disagreement lay in the N-terminal extracellular domain, with AF predicting greater secondary structure than the I-TASSER model. Around the drug-binding pocket examined above, AF predicts a smaller and more open binding pocket due to the  $\alpha_5$

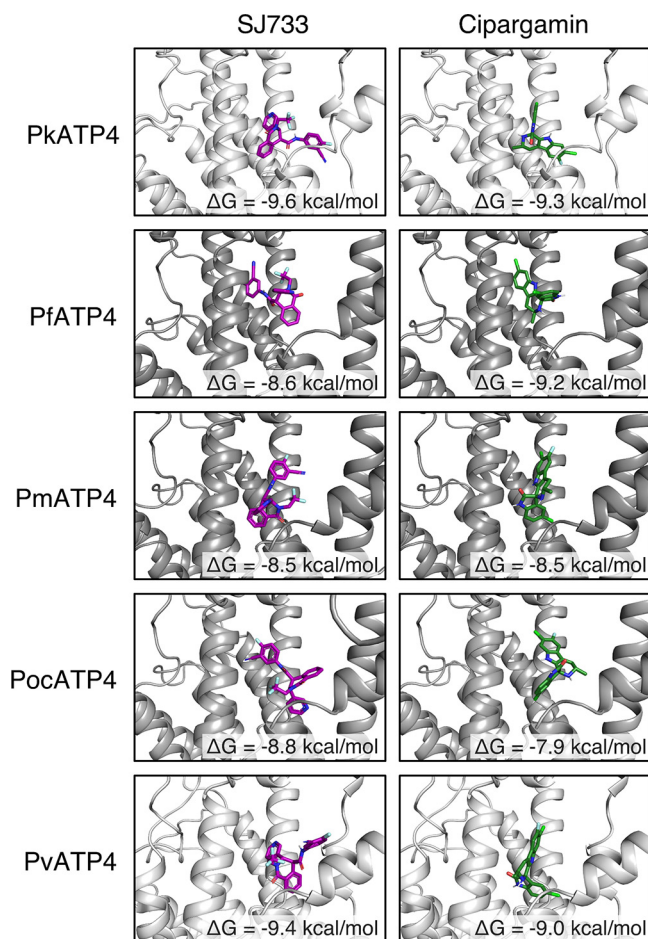


**FIG 6** Structural models of top solutions of SJ733 and cipargamin docked to ATP4 orthologues. Solution structures of SJ733 (purple molecules, left column) and cipargamin (green molecules, right column) docked to model structures of ATP4 orthologues produced by AutoDock Vina. The inset label refers to the AutoDock-calculated free energy ( $\Delta G$ ) dissipated during formation of each protein-drug complex in kilocalories per mole.  $|\Delta\Delta G| > 1 \text{ kcal/mol}$  indicates a significant perturbation in binding.

and  $\alpha_6$  helices, which define the front of the pocket, being pushed downwards by  $\sim 6 \text{ \AA}$ . pLDDT confidence scores in the pocket range from 60 to 89 (low to confident) (Fig. S2). We used the AF structure as a threading template to resolve a new model structure, PocATP4\_AF. PocATP4 was selected because the PfATP4<sup>OR</sup> and PocATP4<sup>OR</sup> lines consistently defined the maximum and minimum EC<sub>50</sub> values to all three ATP4-targeting drugs. We noted similar alignment and structural features with these AF models as with the I-TASSER models, with no obvious features in the drug-binding pocket that would explain our *in vitro* drug susceptibility results. Dissipated free energies of docking were similar for SJ733 and cipargamin between the orthologues, consistent with no clear concordance between docking energies and the observed *in vitro* drug susceptibilities above.

## DISCUSSION

In this study, we successfully generated a series of transgenic *P. knowlesi* orthologue replacement (OR) lines *in vitro* in which the endogenous *pkatp4* locus was replaced by a recodonized *pkatp4* coding region or the orthologous coding region from *P. falciparum*, *P. malariae*, *P. ovale* subsp. *curtisi*, or *P. vivax*. Each orthologue replacement transgenic line displayed a similar growth pattern to the parental *P. knowlesi* line, and susceptibility data were generated for each antimalarial compound of interest. We found evidence of significant orthologue-specific differences in parasite susceptibility to three chemically unrelated

ATP4 inhibitors, but not to comparator drugs, among the *P. knowlesi* OR lines. The PfATP4<sup>OR</sup> transgenic line of *P. knowlesi* was significantly more susceptible than the PkATP4<sup>OR</sup> comparator to cipargamin, PA21A092, and SJ733. In contrast, the PocATP4<sup>OR</sup> transgenic line was significantly less susceptible to these ATP4 inhibitors than the comparator line. The PmATP4<sup>OR</sup> and PvATP4<sup>OR</sup> lines were, however, not significantly different from the control PkATP4<sup>OR</sup> line for two of the three ATP4 inhibitors (Table 1). Despite variation in the resting intracellular sodium concentrations among *P. knowlesi* lines expressing each of the five orthologues, we were able to measure significant differences in the magnitude of rapid, cipargamin-induced Na<sup>+</sup> influx and the maximum increase in [Na<sup>+</sup>]<sub>i</sub>, between the *P. falciparum* OR line and each of the other four lines (Table 2), suggesting a real difference in the immediate functional impact of drug exposure on ATP4. In parallel experiments, cipargamin-induced increase in intracellular pH was observed in all lines, but was not significantly affected by the ATP orthologue present. Taken together, our findings confirm that species-specific susceptibility differences previously observed in rodent malaria and in *ex vivo* studies of human isolates are partly or wholly enshrined in the primary amino acid sequences of the respective ATP4 orthologues (18, 25). Our findings also confirm *P. knowlesi* as an important *in vitro* model for studying drug susceptibility in non-falciparum malaria parasites (24, 34), adding to its recently demonstrated utility for vaccine studies in *P. vivax* (26, 27, 39–42).

In other studies of the susceptibility of human malaria parasites to ATP4 inhibitors, cipargamin was shown to be effective against *P. falciparum* and *P. vivax* in *ex vivo* and *in vivo* studies, whereas the pyrazoleamide PA21A092 was more potent against *P. vivax* (15, 19, 43). However, in our *in vitro* studies, we showed that *P. falciparum* 3D7 was over 6-fold more susceptible than *P. knowlesi* A1-H.1 to the ATP4 inhibitors cipargamin, PA21A092, and SJ733 when tested under identical conditions (24). Furthermore, our recent *ex vivo* drug screens with cipargamin also performed under identical conditions confirmed that *P. falciparum* samples were more susceptible than those of *P. malariae* and *P. ovale* samples (25). The experiments enabled by the orthologue replacement lines have generated EC<sub>50</sub> estimates suggestive of three distinct levels of enzymatic susceptibility (EC<sub>50</sub> of PfATP4<sup>OR</sup> << PmATP4<sup>OR</sup> ≈ PkATP4<sup>OR</sup> ≈ PvATP4 << PocATP4<sup>OR</sup>) and indicate that this appears to be universal for distinct ATP4 inhibitor classes. Future work to extend the panel of ATP4 inhibitors will enable us to examine whether this rank order of susceptibility remains the same or varies for distinct inhibitor structures.

Cipargamin causes a rapid influx in Na<sup>+</sup>, which followed a species-specific pattern, with a clear dichotomy in the magnitude of [Na<sup>+</sup>]<sub>i</sub> flux between the PfATP4<sup>OR</sup> line and the other *P. knowlesi* OR transgenic lines. This suggests a particularly profound functional impact of drug on PfATP4. The use of a single high cipargamin concentration may not be ideal to compare species differences. It may be preferable in future to use a preset multiple of the EC<sub>50</sub> value (e.g., 5× the EC<sub>50</sub> value) considering the wide variability of drug susceptibilities. For example, 100 nM cipargamin represents 60× the PfATP4<sup>OR</sup> EC<sub>50</sub> value but only around 3× the PocATP4<sup>OR</sup> EC<sub>50</sub> value. Alternatively, full dose-response curves for disruption of [Na<sup>+</sup>]<sub>i</sub> regulation could be generated, as described for *P. falciparum* previously (17). Our understanding of these P-type ATPases remains inadequate, as well as how these interact with other cellular processes to regulate intracellular cation concentrations and pH.

Our data represent an important step forward in our understanding of ATP4 inhibitors. Recent phylogenetic analyses place PfATP4 into a distinct subgroup of P-type ATPases called “ATP4-type ATPases” (44). These are restricted to apicomplexan parasites (including *Toxoplasma* and *Plasmodium*) and closely related organisms, such as chromerids and dinoflagellates, and are absent in other eukaryotes (44). Mutations in PfATP4 are associated with resistance to a wide range of novel antimalarial candidates, including spiroindolones, MMV Malaria Box compounds, pyrazoles, and dihydroisoquinolones (15, 18, 19, 21), most of which show minimal toxicity against mammalian cells. The *in silico* modeling relied on a previously determined crystal structure from a rabbit calcium pump and would therefore benefit in the future from availability of the empirically derived structure of an ATP4-type



ATPase from another apicomplexan or closely related organism. Jimenez-Diaz et al. previously used *in silico* modeling based on the rabbit calcium pump to explain species differences in susceptibility to SJ733 between the murine malarial and *P. falciparum* (18). In that study an important 5-amino-acid variant sequence loop was identified near the binding site that may explain the variations in SJ733 susceptibility between species (18). Most of the structural and sequence variations between the ATP4 orthologues were found in the extracellular domain. We could not identify bulkier amino acid side chains in the drug-binding pocket that might be responsible for steric constraints underlying the species differences in susceptibility to cipargamin and SJ733. Dissipated free energies of protein-drug docking did not reveal an orthologue rank order consistent with our *in vitro* observations. The 5-amino-acid sequence identified previously is spatially distant from the nearest atom of SJ733 and cipargamin and does not have the predicted secondary structure. We have been able to supplement this work with the use of AlphaFold structural predictions, and these provided results consistent with the threaded I-TASSER model. From our models, it is not obvious how this short loop mediates the significant differences in drug sensitivity observed for each orthologue, but it could be that species-specific differences in loop rigidity moves the conserved  $\alpha_5$  and  $\alpha_6$  into stabilizing or destabilizing interactions. Critically, the orthologous loop that is most conserved with the sequence in PfATP4 is found in *P. ovale*—the least sensitive ATP4 orthologue. Further work is required to pinpoint key sequence differences responsible for these drug susceptibility differences.

Our findings argue for the exploration of drug efficacy in human clinical trials with arms exposed to multiple-species malaria. The observed differences may reflect only a marginal impact on clinical efficacy for cipargamin: for example, where an  $EC_{50}$  estimate of 40 nM for the PocATP4 orthologue indicates that the drug retains excellent potency, but may mean certain species more easily acquire resistance or may require different dosage regimens. Conversely, it is unlikely that infections with either *P. ovale* subsp. *curtisi* or *P. ovale* subsp. *wallikeri* (these two species are very close relatives, with minimal divergence of “housekeeping” enzyme sequences) would respond well to treatment with either PA21A092 or SJ733, a finding with relevance for malaria treatment in sub-Saharan Africa, where these two species are widely distributed (45). Notably, none of the ATP4 orthologues appeared to result in any reduction in parasite fitness. Previous studies of ATP4 resistance mutations in *P. falciparum* reported variable effects on parasite growth, with some mutations resulting in a fitness cost (18), while other mutations produced no fitness cost (46). In our study, we compared growth of individual lines across only one life cycle duration. Other parasite fitness tests involve pairing wild-type with mutant lines and assessing growth across multiple life cycles (e.g., 20 to 30 days in reference 18). This approach, combining two lines in one culture at the same inoculum and comparing their growth across several growth cycles, may reveal differences in the fitness of different ATP4 orthologues compared to others.

In this study, we utilized the *P. knowlesi* model to explore species differences in ATP4 inhibitor susceptibility that we had identified in previous *in vitro* and *ex vivo* drug susceptibility studies (24, 25). This model has also been used to examine putative *P. vivax* drug resistance genes (42) and to study *P. vivax* malaria vaccine targets (41) and invasion (27). An advantage of using the *P. knowlesi* transfection model over the *P. falciparum* model is that *P. knowlesi* is phylogenetically more closely related to all the human malaria species (particularly *P. vivax*) than *P. falciparum* (33). Also, *P. knowlesi* possesses a more balanced genome AT content (62.5%) than *P. falciparum* and demonstrates transfection efficiency orders of magnitude higher (26, 39, 40). Our genome editing approach also has the key advantage of placing the orthologue gene into the ATP4 locus, directly under the endogenous *P. knowlesi* 5' and 3' untranslated regions (UTRs), providing significant advantages over exogenous episomal constructs or those controlled by generic expression cassettes. Although not used here, the lines generated are also markerless, so can be modified iteratively in future work. Our current analysis used orthologue sequences taken from reference genomes of each of the human infective species—but we still do not know how natural diversity in ATP4 from different species may affect ATP4 inhibitor susceptibility. The role of ATP4 variation identified from population genetics studies in each of the human infective



species can be readily tested using this approach. Similarly, whether orthologue susceptibility and selected *P. falciparum* resistance mutations can interact to further modulate susceptibility in non-falciparum species could be investigated in this way. A limitation of our study is that we did not measure ATP4 orthologue expression or cellular localization in our transfectant lines. This would require antibodies to each orthologue or an appropriate tag, which was beyond the scope of the current study. However, given that ATP4 is essential and the orthologue replacements resulted in normal parasite growth rates, any difference in expression levels in the recodonized ATP4 sequences is likely small. Furthermore, the control recodonization of PkATP4 maintained parental inhibitor susceptibility and the orthologue replacement transgenics recapitulated the species differences observed for the susceptibility of *ex vivo* malaria parasites to cipargamin published by us previously (25).

Our study firmly establishes the existence of species-specific differences in susceptibility of human-infecting *Plasmodium* spp. to ATP4 inhibitors and provides compelling evidence that these differences lie within the primary sequence of the ATP4 protein orthologue in each parasite. We have also shown the enormous potential of *P. knowlesi* as a genetically tractable *in vitro* experimental workhorse for drug susceptibility studies of relevance to all the malaria parasites of humans.

## MATERIALS AND METHODS

**Parasite maintenance, transfection, and dilution cloning.** Human blood from all blood groups was obtained from the United Kingdom National Blood Transfusion Service. *P. knowlesi* is unable to grow in Duffy-negative (Fy<sup>-</sup>) red blood cells (RBCs) (40). Therefore, each new batch of red blood cells was tested first to assess whether they can support the parental *P. knowlesi* line at a normal 3- to 4-fold growth rate before being used to grow the transfectant lines. Parasites were maintained in complete medium, comprising RPMI 1640 (Invitrogen) with the following additions: 2.0 g/L sodium bicarbonate, 4.0 g/L D-glucose, 25 mM HEPES, 0.05 g/L hypoxanthine, 5 g/L AlbuMAX II, 0.025 g/L gentamicin sulfate, 2 mM L-glutamine, and 10% (vol/vol) horse serum (Pan Biotech; P30-0702) as described previously (47). Parasites were synchronized by using gradient centrifugation with 55% Nycodenz (Progen; product 1002424) in RPMI to enrich schizonts, followed by a 2-h incubation with 4-[7-[(dimethylamino)methyl]-2-(4-fluorophenyl)imidazo[1,2-a]pyridin-3-yl]pyrimidin-2-amine (compound 2), which inhibits parasite egress (48).

Tightly synchronized mature schizonts were transfected as described previously using the Amaxa 4D electroporator (Lonza) and the P3 primary cell 4D Nucleofector X kit L (Lonza; product V4XP-3024) (40). Ten microliters of DNA, including 20  $\mu$ g pCas9/sg\_PkATP4 plasmid and 40  $\mu$ g repair template pDonor\_ATP4<sup>OR</sup> (containing the recodonized orthologue PfATP4, PkATP4, PmATP4, PocATP4, or PvATP4), was used for transfections to generate ATP4 transgenic lines. After 24 h, and at daily intervals for 5 days, the medium was replaced with fresh medium containing 100 nM pyrimethamine (Sigma; product P7771). Parasite clones were obtained by limiting dilution. Parasites were diluted to 0.3 parasite/100  $\mu$ L, and 100  $\mu$ L of 2% hematocrit culture was transferred to 96 flat-bottom plates in culture medium containing 2 mM L-GlutaMAX (Gibco; product 35050). After 7 days, the plate was screened for plaques in an assay modified from *P. falciparum* (49). Plaque-positive cultures were transferred to 24-well plates containing 1 mL medium with 2% hematocrit and used for genotyping when parasites appeared in culture.

**Cloning of transfection plasmids.** For cloning of pCas9/sg\_ATP4 plasmids, two *P. knowlesi* target-specific 20-bp guide sequences were chosen with the Protospacer software (<http://www.protospacer.com/>) (50) (GCAGAAGGCTTTGAGAGTTC and TGTTCTGAAGTTACCCGCTG), with off-target scores of 0.0103 and 0.0105. Subsequently, each guide was inserted into the BtgZI linearized pCas9/sg plasmid by In-Fusion cloning (TaKaRa) using forward oligonucleotide TTACAGTATATTATT(N20)GTTTTAGAGCTAGAA and reverse oligonucleotide TTCTAGCTCTAAAAC(N20)AATAATATACTGTAA as described before (26, 51).

For cloning the donor plasmid pDonor\_ATP4, homology regions were amplified from *Plasmodium knowlesi* parental A1-H.1 genomic DNA by using CloneAmp polymerase (TaKaRa). The 5' homology region was amplified with forward oligonucleotide atatgCCGCGGTATACAAGAAGAAAATAGGCCTTTGAATAAG and reverse oligonucleotide atatgaACTAGTAACCTTTTAGGAAAACACGGAAAGTGAAAAAAG leading to a 719-bp fragment of PkATP4 5' UTR. The 3' homology region was amplified with forward oligonucleotide atatggaGCGCGGCTGCAGAGGTGGAATAATCATCACTTGG and reverse oligonucleotide atatggaCCATGGGCGGTATACCCATACGGCGC generating a 748-bp region of the PkATP4 3' UTR (lower case letters are random spacer bases and underlined indicate the restriction site sequences.). The homology regions were introduced into a plasmid backbone with SacI/Spel and NotI/NcoI restriction sites. Sequences of SERCA-type Ca<sup>2+</sup>-transporting P-ATPase orthologues were retrieved from PlasmoDB (<https://plasmodb.org/>): PkATP4 (PKNH\_1312000), PfATP4 (Pf3D7\_1211900), PmATP4 (PmUG01\_13021900), PocATP4 (PocGH01\_13021900), and PvATP4 (PvP01\_1311100). Recodonized synthetic sequences representing each orthologue coding region were obtained from GeneArt and were designed to be flanked by Spel and NotI restriction sites, permitting insertion between the homology regions following Spel/NotI restriction digest. Each synthetic sequence was thus inserted into a plasmid, flanked with the 5' and 3' UTRs of *pkatp4* as homologous repair templates (pDonor\_*pkatp4*). Together with a plasmid containing the Cas9 endonuclease, one of two guide RNAs and a positive/negative selection marker cassette, each pDonor plasmid was transfected into

synchronous late stage schizonts of *P. knowlesi* A1-H.1 strain as previously described (22). After genotyping, parasite lines were cloned by limiting dilution, resulting in 50% to 100% of the clones with successful replacement.

Plasmids for transfection were prepared by Midi-preps (Qiagen) and ethanol precipitated. The DNA pellet was washed twice with 70% ethanol and resuspended in sterile Tris-EDTA (TE) buffer.

**DNA analysis.** Genomic DNA from transfected parasite lines was extracted (Qiagen) and analyzed by PCR with SapphireAmp Fast PCR master mix (TaKaRa; product RR530B) using the following conditions: 1 min at 94°C, then 34 cycles of 5 s at 98°C, 5 s at 62°C and 10 s/kb at 72°C. The diagnostic oligonucleotides for the WT PkATP4 locus are forward oligonucleotide CTTCTAAGGGGTCTAAGAGAGGTAG and reverse oligonucleotide GTGTGTGCACTGCTAGGTACGG. The forward oligonucleotides for integration are as follows: PfATP<sup>OR</sup>, CCCTGCTGAACCTGTTTCTGGAC; PkATP4<sup>OR</sup> and PocATP4<sup>OR</sup>, CTCCACATGCATCCCCGGCA; PmATP<sup>OR</sup>, GAACACCACATGCTGCTGTGGTG; and PvATP4<sup>OR</sup>, CATTCTGGCCACATGCATCCCT. The reverse oligonucleotide for all orthologues was GTGTGTGCACTGCTAGGTACGG. The oligonucleotides for independent locus PkMTIP are forward oligonucleotide CCCGGGGCGTTTTCGCGTATCTGCGCTTTTTC and reverse oligonucleotide CCTAGGGGACAATATATCCTCACAGAAACAATTG.

**Parasite multiplication rate assays.** In the flow cytometry-based parasite multiplication rate assay, the fold increase in parasitemia following one round of asexual growth is measured. Purified schizonts were set up in technical duplicate cultures with human RBCs, at a 2% hematocrit and ~0.5% parasitemia in 24-well plates. Parasitemia was measured with a flow cytometry (fluorescence-activated cell sorter [FACS]) based assay before and after incubation at 37°C in a gassed chamber for 24 h. Samples were stained for 30 min with SYBR green I (Thermo Fisher Scientific; product S7563) and counted with the Attune flow cytometer (Thermo Fisher Scientific).

**Growth inhibition assay.** The ATP4 inhibitors cipargamin, PA21A092, and SJ733, as well as the established antimalarials chloroquine and dihydroartemisinin, were supplied by the Medicines for Malaria Venture, Geneva, Switzerland. Chloroquine stocks were prepared in sterile distilled water, but all other stocks were prepared in dimethyl sulfoxide (DMSO).

Drug susceptibility of *P. knowlesi* parental and transgenic parasite lines was assessed as described previously with parasites exposed to the serial dilutions of the drugs for one complete life cycle (27 h) (24).

Parasite viability was determined using the SYBR green I fluorescence method (52, 53) as described elsewhere (24). Fluorescence was read using either a Spectramax M3 or iD5 microplate reader (Molecular Devices) at the 520-nm wavelength after excitation at 490 nm.

**Parasite [Na<sup>+</sup>]<sub>i</sub> and pH<sub>i</sub> measurements.** For both [Na<sup>+</sup>]<sub>i</sub> and pH<sub>i</sub> measurements, mature stage trophozoite parasites (36 to 40 h postinvasion for *P. falciparum*, 20 to 23 h postinvasion for *P. knowlesi*) were first isolated from their erythrocytes through treatment with saponin (0.05% [wt/vol]) (35).

The pH-sensitive fluorescent dye BCECF [2',7'-bis-(2-carboxyethyl)-5-(and-6)-carboxyfluorescein] (Biotium; product 51011) was used to measure the cytosolic pH of the *P. falciparum* 3D7 line and the *P. knowlesi* parental (A1-H.1) and transfectant lines. Saponin-isolated trophozoite parasites were loaded with the acetoxymethyl ester of BCECF as described before (35). Thereafter, the parasites were suspended in physiological saline (120 mM NaCl, 5 mM KCl, 25 mM HEPES, 20 mM D-glucose, and 1 mM MgCl<sub>2</sub> [pH 7.1]) in the presence or absence of various concentrations of ATP4 inhibitors in a 96-well microtiter plate (200 μL of parasite suspension per well). After being loaded into a 96-well microtiter plate, the fluorescence was measured at a wavelength of 520 nm after excitation at both 440 nm and 490 nm using a Spectramax M3 microplate reader (Molecular Devices) in a temperature-controlled chamber at 37°C.

For each experiment, a pH calibration was performed. Briefly, the BCECF-loaded parasites were suspended in a high-K<sup>+</sup> saline (130 mM KCl, 25 mM HEPES, 20 mM D-glucose, and 20 mM MgCl<sub>2</sub>) at pH values of 6.8, 7.1, and 7.8. To this was added 15 μM nigericin (Tocris Bioscience; product 4312) which sets the intracellular pH to that of the surrounding saline. A linear regression can then be plotted between the calibration pH values and the intracellular fluorescence ratios (490 nm/440 nm). Then, for the experimental samples, this linear equation is used to convert fluorescence into pH units.

Intracellular sodium ([Na<sup>+</sup>]<sub>i</sub>) was measured using the Na<sup>+</sup>-sensitive fluorescent dye SBFI (Thermo Fisher Scientific; product S1263). Saponin-isolated trophozoites were loaded with the acetoxymethyl ester of SBFI as described by others (17). Thereafter, SBFI-loaded parasites were resuspended in physiological saline (as described above) at 37°C in the presence or absence of the ATP4 inhibitors. Calibration curves were set up using SBFI-loaded parasites suspended in calibration buffers with [Na<sup>+</sup>] concentrations between 0 and 130 mM (pH 7.3) containing 110 mM Na<sup>+</sup>/K<sup>+</sup> gluconate, 30 mM Na<sup>+</sup>/K<sup>+</sup> Cl, 1.2 mM CaCl<sub>2</sub>, 0.6 mM MgCl<sub>2</sub>, and 10 mM HEPES and the ionophore gramicidin D (17).

The parasites were loaded into a 96-well microtiter plate, and the fluorescence was measured at a wavelength of 515 nm after successive excitation at 340 nm and 380 nm. Calibration was performed as described previously to compare the relationship between the 340-nm/380-nm ratio and intracellular sodium (54, 55). The rates of increase in [Na<sup>+</sup>]<sub>i</sub> observed 10 min after the addition of 100 nM cipargamin were calculated by fitting a linear regression equation ( $y = mx + b$ ) to the data. The slope ( $m$ ) represents the rate of change, and  $b$  represents the intercept. The maximum change in [Na<sup>+</sup>]<sub>i</sub> after the addition of cipargamin was calculated by subtracting the minimum value for [Na<sup>+</sup>]<sub>i</sub> (i.e., immediately before the addition of cipargamin) from the highest [Na<sup>+</sup>]<sub>i</sub> achieved within the first 10 min of cipargamin exposure.

**Molecular modeling and docking.** Molecular models of PfATP4 were constructed using the molecular threading algorithm I-TASSER (56). Briefly, the amino acid sequence was modeled *de novo* and separately threaded through the crystal structure of the *Oryctolagus cuniculus* calcium pump (PDB no. 2DQS), a transmembrane (TM) Ca<sup>2+</sup> ATPase found to have similar predicted TM domain structure, a technique used previously by Jimenez-Diaz et al. (18). The resulting molecular models of PfATP4 were then validated for structural

similarity by alignment with the Jimenez-Diaz model and subsequently used as a threading template for the remaining *P. knowlesi*, *P. vivax*, *P. malariae*, and *P. ovale curtisi* ATP4 sequences.

The molecular structures of SJ733 and cipargamin were then docked to these structures using AutoDock Vina 1.1.2 over the entire solvent-exposed surface area as well as within a docking grid (22.5 Å in each dimension) constrained to the SJ733 binding pocket identified by Jimenez-Diaz et al. (18). Docking SJ733 to PfATP4 over the entire protein surface area reidentified the binding pocket identified by Jimenez-Diaz et al., and thus the constrained docking approach was used for the other species to investigate a greater number of docking configurations for each ATP4 homolog. The intrinsic Vina scoring function (57) was used to calculate and compare the dissipated free energy of the top docking solution for each structure.

Visualizations of the molecular models and docked structures were prepared using Chimera (58) and PyMol (version 2.4.0) (Schrödinger).

**Statistical analysis.** Data from the orthologue replacement lines were compared using ordinary one-way analysis of variance (ANOVA) with Dunnett's multiple-comparison test to determine differences of the orthologue replacement lines compared to the PkATP4<sup>OR</sup> line.

## SUPPLEMENTAL MATERIAL

Supplemental material is available online only.

**FIG S1**, PDF file, 0.2 MB.

**FIG S2**, PDF file, 0.3 MB.

**TABLE S1**, DOCX file, 0.01 MB.

**TABLE S2**, DOCX file, 0.01 MB.

## ACKNOWLEDGMENTS

This work is supported by an MRC Career Development Award (MR/M021157/1) jointly funded by the U.K. Medical Research Council and Department for International Development (R.W.M. and F.M.) and a Medicines for Malaria Venture grant (MMV RD/15/0017) awarded to D.A.v.S.

We thank the laboratories of R. Kip Guy, Joseph DeRisi, and Andrej Sali for providing structural models of ATP4 from the original publication by Jimenez-Diaz et al. (18) for comparison and validation of the models described here.

F.M. contributed Formal Analysis, Validation, Investigation, Visualization, Methodology, Writing – Original Draft, Writing – Review & Editing; C.J.S. contributed Study Design, Funding Acquisition, Writing – Review & Editing; R.H. contributed Formal Analysis, Validation, Investigation, Visualization, Methodology, Writing – Original Draft, Writing – Review & Editing; R.W.M. contributed Conceptualization, Supervision, Funding Acquisition, Writing – Review & Editing; D.A.v.S. contributed Conceptualization, Funding Acquisition, Project Administration, Data Curation, Formal Analysis, Validation, Investigation, Visualization, Methodology, Writing – Original Draft, Writing – Review & Editing; B.B. contributed Project Management from MMV, Writing – Review & Editing; D.L. contributed Project Supervision from MMV, Writing – Review & Editing.

B.B. was and D.L. is an employee of the funder, the Medicines for Malaria Venture. All other authors declare no conflict of interest.

## REFERENCES

- World Health Organization. 2021. World malaria report 2021. <https://www.who.int/teams/global-malaria-programme/reports/world-malaria-report-2021>.
- World Health Organization. 2020. World malaria report 2020: 20 years of global progress and challenges. <https://www.who.int/teams/global-malaria-programme/reports/world-malaria-report-2020>.
- Rajahram GS, Cooper DJ, William T, Grigg MJ, Anstey NM, Barber BE. 2019. Deaths from *Plasmodium knowlesi* malaria: case series and systematic review. *Clin Infect Dis* 69:1703–1711. <https://doi.org/10.1093/cid/ciz011>.
- World Health Organization. 2015. Guidelines for the treatment of malaria, 3rd ed. World Health Organization, Geneva, Switzerland.
- Amaratunga C, Lim P, Suon S, Sreng S, Mao S, Sopha C, Sam B, Dek D, Try V, Amato R, Blessborn D, Song L, Tullo GS, Fay MP, Anderson JM, Tarning J, Fairhurst RM. 2016. Dihydroartemisinin-piperazine resistance in *Plasmodium falciparum* malaria in Cambodia: a multisite prospective cohort study. *Lancet Infect Dis* 16:357–365. [https://doi.org/10.1016/S1473-3099\(15\)00487-9](https://doi.org/10.1016/S1473-3099(15)00487-9).
- Saunders DL, Vanachayangkul P, Lon C, US Army Malaria Research Program, National Center for Parasitology, Entomology, and Malaria Control (CNM), Royal Cambodian Armed Forces. 2014. Dihydroartemisinin-piperazine failure in Cambodia. *N Engl J Med* 371:484–485. <https://doi.org/10.1056/NEJMc1403007>.
- Spring MD, Lin JT, Manning JE, Vanachayangkul P, Somethy S, Bun R, Se Y, Chann S, Ittiverakul M, Sia-ngam P, Kuntawunginn W, Arsanok M, Buathong M, Chaorattanakawee S, Gosi P, Ta-aksorn W, Chanarat N, Sundrakes S, Kong N, Heng TK, Nou S, Teja-isavadharm P, Pichyangkul S, Phann ST, Balasubramanian S, Juliano JJ, Meshnick SR, Chour CM, Prom S, Lanteri CA, Lon C, Saunders DL. 2015. Dihydroartemisinin-piperazine failure associated with a triple mutant including kelch13 C580Y in Cambodia: an observational cohort study. *Lancet Infect Dis* 15:683–691. [https://doi.org/10.1016/S1473-3099\(15\)70049-6](https://doi.org/10.1016/S1473-3099(15)70049-6).
- Balikagala B, Fukuda N, Ikeda M, Katuro OT, Tachibana SI, Yamauchi M, Opio W, Emoto S, Anywar DA, Kimura E, Palacpac NMQ, Odongo-Aginya EI, Ogwang M, Horii T, Mita T. 2021. Evidence of artemisinin-resistant malaria in Africa. *N Engl J Med* 385:1163–1171. <https://doi.org/10.1056/NEJMoa2101746>.
- Uwimana A, Umulisa N, Venkatesan M, Svigel SS, Zhou Z, Munyaneza T, Habimana RM, Rucogoza A, Moriarty LF, Sandford R, Piercefield E, Goldman I,

- Ezema B, Talundzic E, Pacheco MA, Escalante AA, Ngamije D, Mangala JN, Kabera M, Munguti K, Murindahabi M, Brieger W, Musanabaganwa C, Mutesa L, Udhayakumar V, Mbituyumuremyi A, Halsey ES, Lucchi NW. 2021. Association of *Plasmodium falciparum* kelch13 R561H genotypes with delayed parasite clearance in Rwanda: an open-label, single-arm, multicentre, therapeutic efficacy study. *Lancet Infect Dis* 21:1120–1128. [https://doi.org/10.1016/S1473-3099\(21\)00142-0](https://doi.org/10.1016/S1473-3099(21)00142-0).
10. White NJ. 2021. Emergence of artemisinin-resistant *Plasmodium falciparum* in East Africa. *N Engl J Med* 385:1231–1232. <https://doi.org/10.1056/NEJMe2110659>.
  11. Gamo FJ, Sanz LM, Vidal J, de Cozar C, Alvarez E, Lavandera JL, Vanderwall DE, Green DV, Kumar V, Hasan S, Brown JR, Peishoff CE, Cardon LR, Garcia-Bustos JF. 2010. Thousands of chemical starting points for antimalarial lead identification. *Nature* 465:305–310. <https://doi.org/10.1038/nature09107>.
  12. Guiguemde WA, Shelat AA, Bouck D, Duffy S, Crowther GJ, Davis PH, Smithson DC, Connelly M, Clark J, Zhu F, Jimenez-Diaz MB, Martinez MS, Wilson EB, Tripathi AK, Gut J, Sharlow ER, Bathurst I, El Mazouni F, Fowble JW, Forquer I, McGinley PL, Castro S, Angulo-Barturen I, Ferrer S, Rosenthal PJ, Derisi JL, Sullivan DJ, Lazo JS, Roos DS, Riscoe MK, Phillips MA, Rathod PK, Van Voorhis WC, Avery VM, Guy RK. 2010. Chemical genetics of *Plasmodium falciparum*. *Nature* 465:311–315. <https://doi.org/10.1038/nature09099>.
  13. Plouffe D, Brinker A, McNamara C, Henson K, Kato N, Kuhen K, Nagle A, Adrian F, Matzen JT, Anderson P, Nam TG, Gray NS, Chatterjee A, Janes J, Yan SF, Trager R, Caldwell JS, Schultz PG, Zhou Y, Winzeler EA. 2008. *In silico* activity profiling reveals the mechanism of action of antimalarials discovered in a high-throughput screen. *Proc Natl Acad Sci U S A* 105:9059–9064. <https://doi.org/10.1073/pnas.0802982105>.
  14. Phillips MA, Rathod PK. 2010. *Plasmodium* dihydroorotate dehydrogenase: a promising target for novel anti-malarial chemotherapy. *Infect Disord Drug Targets* 10:226–239. <https://doi.org/10.2174/187152610791163336>.
  15. Rottmann M, McNamara C, Yeung BK, Lee MC, Zou B, Russell B, Seitz P, Plouffe DM, Dharia NV, Tan J, Cohen SB, Spencer KR, Gonzalez-Paez GE, Lakshminarayana SB, Goh A, Suwanarusk R, Jegla T, Schmitt EK, Beck HP, Brun R, Nosten F, Renia L, Dartois V, Keller TH, Fidock DA, Winzeler EA, Diagona TT. 2010. Spiroindolones, a potent compound class for the treatment of malaria. *Science* 329:1175–1180. <https://doi.org/10.1126/science.1193225>.
  16. Flannery EL, Chatterjee AK, Winzeler EA. 2013. Antimalarial drug discovery—approaches and progress towards new medicines. *Nat Rev Microbiol* 11:849–862. <https://doi.org/10.1038/nrmicro3138>.
  17. Spillman NJ, Allen RJ, McNamara CW, Yeung BK, Winzeler EA, Diagona TT, Kirk K. 2013. Na<sup>+</sup> regulation in the malaria parasite *Plasmodium falciparum* involves the cation ATPase PfATP4 and is a target of the spiroindolone antimalarials. *Cell Host Microbe* 13:227–237. <https://doi.org/10.1016/j.chom.2012.12.006>.
  18. Jimenez-Diaz MB, Ebert D, Salinas Y, Pradhan A, Lehane AM, Myrand-Lapierre ME, O'Loughlin KG, Shackelford DM, Justino de Almeida M, Carrillo AK, Clark JA, Dennis AS, Diep J, Deng X, Duffy S, Endsley AN, Fedewa G, Guiguemde WA, Gomez MG, Holbrook G, Horst J, Kim CC, Liu J, Lee MC, Matheny A, Martinez MS, Miller G, Rodriguez-Alejandre A, Sanz L, Sigal M, Spillman NJ, Stein PD, Wang Z, Zhu F, Waterson D, Knapp S, Shelat A, Avery VM, Fidock DA, Gamo FJ, Charman SA, Mirsalis JC, Ma H, Ferrer S, Kirk K, Berriman M, Kortagere S, Burrows J, Fan E, Bergman LW. 2014. (+)-SJ733, a clinical candidate for malaria that acts through ATP4 to induce rapid host-mediated clearance of *Plasmodium*. *Proc Natl Acad Sci U S A* 111:E5455–E5462.
  19. Vaidya AB, Morrisey JM, Zhang Z, Das S, Daly TM, Otto TD, Spillman NJ, Wyvrat M, Siegl P, Marfurt J, Wirjanata G, Sebayang BF, Price RN, Chatterjee A, Nagle A, Stasiak M, Charman SA, Angulo-Barturen I, Ferrer S, Belen Jimenez-Diaz M, Martinez MS, Gamo FJ, Avery VM, Ruecker A, Delves M, Kirk K, Berriman M, Kortagere S, Burrows J, Fan E, Bergman LW. 2014. Pyrazoleamide compounds are potent antimalarials that target Na<sup>+</sup> homeostasis in intraerythrocytic *Plasmodium falciparum*. *Nat Commun* 5:5521. <https://doi.org/10.1038/ncomms6521>.
  20. Dennis ASM, Rosling JEO, Lehane AM, Kirk K. 2018. Diverse antimalarials from whole-cell phenotypic screens disrupt malaria parasite ion and volume homeostasis. *Sci Rep* 8:8795. <https://doi.org/10.1038/s41598-018-26819-1>.
  21. Lehane AM, Ridgway MC, Baker E, Kirk K. 2014. Diverse chemotypes disrupt ion homeostasis in the malaria parasite. *Mol Microbiol* 94:327–339. <https://doi.org/10.1111/mmi.12765>.
  22. Ganesan SM, Falla A, Goldfless SJ, Nasamu AS, Niles JC. 2016. Synthetic RNA-protein modules integrated with native translation mechanisms to control gene expression in malaria parasites. *Nat Commun* 7:10727. <https://doi.org/10.1038/ncomms10727>.
  23. Krishna S, Woodrow C, Webb R, Penny J, Takeyasu K, Kimura M, East JM. 2001. Expression and functional characterization of a *Plasmodium falciparum* Ca<sup>2+</sup>-ATPase (PfATP4) belonging to a subclass unique to apicomplexan organisms. *J Biol Chem* 276:10782–10787. <https://doi.org/10.1074/jbc.M010554200>.
  24. van Schalkwyk DA, Blasco B, Davina NR, Liew JWK, Amir A, Lau YL, Leroy D, Moon RW, Sutherland CJ. 2019. *Plasmodium knowlesi* exhibits distinct *in vitro* drug susceptibility profiles from those of *Plasmodium falciparum*. *Int J Parasitol Drugs Drug Resist* 9:93–99. <https://doi.org/10.1016/j.ijpddr.2019.02.004>.
  25. van Schalkwyk DA, Moon RW, Duffey M, Leroy D, Sutherland CJ. 2021. *Ex vivo* susceptibility to new antimalarial agents differs among human-infecting *Plasmodium* species. *Int J Parasitol Drugs Drug Resist* 17:5–11. <https://doi.org/10.1016/j.ijpddr.2021.07.002>.
  26. Mohring F, Hart MN, Rawlinson TA, Henrici R, Charleston JA, Diez Benavente E, Patel A, Hall J, Almond N, Campino S, Clark TG, Sutherland CJ, Baker DA, Draper SJ, Moon RW. 2019. Rapid and iterative genome editing in the malaria parasite *Plasmodium knowlesi* provides new tools for *P vivax* research. *eLife* 8:e45829. <https://doi.org/10.7554/eLife.45829>.
  27. Rawlinson TA, Barber NM, Mohring F, Cho JS, Kosaisavee V, Gerard SF, Alanine DGW, Labbe GM, Elias SC, Silk SE, Quinkert D, Jin J, Marshall JM, Payne RO, Minassian AM, Russell B, Renia L, Nosten FH, Moon RW, Higgins MK, Draper SJ. 2019. Structural basis for inhibition of *Plasmodium vivax* invasion by a broadly neutralizing vaccine-induced human antibody. *Nat Microbiol* 4:1497–1507. <https://doi.org/10.1038/s41564-019-0462-1>.
  28. Bermudez M, Moreno-Perez DA, Arevalo-Pinzon G, Curtidor H, Patarroyo MA. 2018. *Plasmodium vivax in vitro* continuous culture: the spoke in the wheel. *Malar J* 17:301. <https://doi.org/10.1186/s12936-018-2456-5>.
  29. Auburn S, Bohme U, Steinbiss S, Trimarsanto H, Hostetler J, Sanders M, Gao Q, Nosten F, Newbold CI, Berriman M, Price RN, Otto TD. 2016. A new *Plasmodium vivax* reference sequence with improved assembly of the subtelomeres reveals an abundance of pir genes. *Wellcome Open Res* 1:4. <https://doi.org/10.12688/wellcomeopenres.9876.1>.
  30. Bohme U, Otto TD, Sanders M, Newbold CI, Berriman M. 2019. Progression of the canonical reference malaria parasite genome from 2002–2019. *Wellcome Open Res* 4:58. <https://doi.org/10.12688/wellcomeopenres.15194.2>.
  31. Gardner MJ, Hall N, Fung E, White O, Berriman M, Hyman RW, Carlton JM, Pain A, Nelson KE, Bowman S, Paulsen IT, James K, Eisen JA, Rutherford K, Salzberg SL, Craig A, Kyes S, Chan MS, Nene V, Shallom SJ, Suh B, Peterson J, Angiuoli S, Pertea M, Allen J, Selengut J, Haft D, Mather MW, Vaidya AB, Martin DM, Fairlamb AH, Fraunholz MJ, Roos DS, Ralph SA, McFadden GI, Cummings LM, Subramanian GM, Mungall K, Venter JC, Carucci DJ, Hoffman SL, Newbold C, Davis RW, Fraser CM, Barrell B. 2002. Genome sequence of the human malaria parasite *Plasmodium falciparum*. *Nature* 419:498–511. <https://doi.org/10.1038/nature01097>.
  32. Pain A, Bohme U, Berry AE, Mungall K, Finn RD, Jackson AP, Mourier T, Mistry J, Pasini EM, Aslett MA, Balasubramanian S, Borgwardt K, Brooks K, Carret C, Carver TJ, Cherevach I, Chillingworth T, Clark TG, Galinski MR, Hall N, Harper D, Harris D, Hauser H, Ivens A, Janssen CS, Keane T, Larke N, Lapp S, Marti M, Moule S, Meyer IM, Ormond D, Peters N, Sanders M, Sanders S, Sargeant TJ, Simmonds S, Smith F, Squares R, Thurston S, Tivey AR, Walker D, White B, Zuiderwijk E, Churcher C, Quail MA, Cowman AF, Turner CM, Rajandream MA, Kocken CH, et al. 2008. The genome of the simian and human malaria parasite *Plasmodium knowlesi*. *Nature* 455:799–803. <https://doi.org/10.1038/nature07306>.
  33. Rutledge GG, Bohme U, Sanders M, Reid AJ, Cotton JA, Maiga-Ascofare O, Djimde AA, Apinjoh TO, Amenga-Etego L, Manske M, Barnwell JW, Renaud F, Ollomo B, Prugnolle F, Anstey NM, Auburn S, Price RN, McCarthy JS, Kwiatkowski DP, Newbold CI, Berriman M, Otto TD. 2017. *Plasmodium malariae* and *P. ovale* genomes provide insights into malaria parasite evolution. *Nature* 542:101–104. <https://doi.org/10.1038/nature21038>.
  34. van Schalkwyk DA, Moon RW, Blasco B, Sutherland CJ. 2017. Comparison of the susceptibility of *Plasmodium knowlesi* and *Plasmodium falciparum* to antimalarial agents. *J Antimicrob Chemother* 72:3051–3058. <https://doi.org/10.1093/jac/dkx279>.
  35. Saliba KJ, Kirk K. 1999. pH regulation in the intracellular malaria parasite, *Plasmodium falciparum*. H<sup>+</sup> extrusion via a V-type H<sup>+</sup>-ATPase. *J Biol Chem* 274:33213–33219. <https://doi.org/10.1074/jbc.274.47.33213>.
  36. van Schalkwyk DA, Chan XW, Misiano P, Gagliardi S, Farina C, Saliba KJ. 2010. Inhibition of *Plasmodium falciparum* pH regulation by small molecule indole derivatives results in rapid parasite death. *Biochem Pharmacol* 79:1291–1299. <https://doi.org/10.1016/j.bcp.2009.12.025>.



37. Spillman NJ, Allen RJ, Kirk K. 2008. Acid extrusion from the intraerythrocytic malaria parasite is not via a Na<sup>+</sup>/H<sup>+</sup> exchanger. *Mol Biochem Parasitol* 162:96–99. <https://doi.org/10.1016/j.molbiopara.2008.07.001>.
38. Jumper J, Evans R, Pritzel A, Green T, Figurnov M, Ronneberger O, Tunyasuvunakool K, Bates R, Zidek A, Potapenko A, Bridgland A, Meyer C, Kohl SAA, Ballard AJ, Cowie A, Romera-Paredes B, Nikolov S, Jain R, Adler J, Back T, Petersen S, Reiman D, Clancy E, Zielinski M, Steinegger M, Pacholska M, Berghammer T, Bodenstein S, Silver D, Vinyals O, Senior AW, Kavukcuoglu K, Kohli P, Hassabis D. 2021. Highly accurate protein structure prediction with AlphaFold. *Nature* 596:583–589. <https://doi.org/10.1038/s41586-021-03819-2>.
39. Gruring C, Moon RW, Lim C, Holder AA, Blackman MJ, Duraisingh MT. 2014. Human red blood cell-adapted *Plasmodium knowlesi* parasites: a new model system for malaria research. *Cell Microbiol* 16:612–620. <https://doi.org/10.1111/cmi.12275>.
40. Moon RW, Hall J, Rangkuti F, Ho YS, Almond N, Mitchell GH, Pain A, Holder AA, Blackman MJ. 2013. Adaptation of the genetically tractable malaria pathogen *Plasmodium knowlesi* to continuous culture in human erythrocytes. *Proc Natl Acad Sci U S A* 110:531–536. <https://doi.org/10.1073/pnas.1216457110>.
41. Ndegwa DN, Kundu P, Hostetler JB, Marin-Menendez A, Sanderson T, Mwakali K, Verzier LH, Coyle R, Adjalley S, Rayner JC. 2021. Using *Plasmodium knowlesi* as a model for screening *Plasmodium vivax* blood-stage malaria vaccine targets reveals new candidates. *PLoS Pathog* 17:e1008864. <https://doi.org/10.1371/journal.ppat.1008864>.
42. Verzier LH, Coyle R, Singh S, Sanderson T, Rayner JC. 2019. *Plasmodium knowlesi* as a model system for characterising *Plasmodium vivax* drug resistance candidate genes. *PLoS Negl Trop Dis* 13:e0007470. <https://doi.org/10.1371/journal.pntd.0007470>.
43. White NJ, Pukrittayakamee S, Phyo AP, Rueangweerayut R, Nosten F, Jittamala P, Jeeyapant A, Jain JP, Lefevre G, Li R, Magnusson B, Diagana TT, Leong FJ. 2014. Spiroindolone KAE609 for falciparum and vivax malaria. *N Engl J Med* 371:403–410. <https://doi.org/10.1056/NEJMoa1315860>.
44. Lehane AM, Dennis ASM, Bray KO, Li D, Rajendran E, McCoy JM, McArthur HM, Winterberg M, Rahimi F, Tonkin CJ, Kirk K, van Dooren GG. 2019. Characterization of the ATP4 ion pump in *Toxoplasma gondii*. *J Biol Chem* 294:5720–5734. <https://doi.org/10.1074/jbc.RA118.006706>.
45. Sutherland CJ, Tanomsing N, Nolder D, Oguike M, Jennison C, Pukrittayakamee S, Dolecek C, Hien TT, do Rosario VE, Arez AP, Pinto J, Michon P, Escalante AA, Nosten F, Burke M, Lee R, Blaze M, Otto TD, Barnwell JW, Pain A, Williams J, White NJ, Day NP, Snounou G, Lockhart PJ, Chiodini PL, Imwong M, Polley SD. 2010. Two nonrecombining sympatric forms of the human malaria parasite *Plasmodium ovale* occur globally. *J Infect Dis* 201:1544–1550. <https://doi.org/10.1086/652240>.
46. Flannery EL, McNamara CW, Kim SW, Kato TS, Li F, Teng CH, Gagaring K, Manary MJ, Barboa R, Meister S, Kuhen K, Vinetz JM, Chatterjee AK, Winzeler EA. 2015. Mutations in the P-type cation-transporter ATPase 4, PfATP4, mediate resistance to both aminopyrazole and spiroindolone antimalarials. *ACS Chem Biol* 10:413–420. <https://doi.org/10.1021/cb500616x>.
47. Moon RW, Sharaf H, Hastings CH, Ho YS, Nair MB, Rchiad Z, Knuepfer E, Ramaprasad A, Mohring F, Amir A, Yusuf NA, Hall J, Almond N, Lau YL, Pain A, Blackman MJ, Holder AA. 2016. Normocyte-binding protein required for human erythrocyte invasion by the zoonotic malaria parasite *Plasmodium knowlesi*. *Proc Natl Acad Sci U S A* 113:7231–7236. <https://doi.org/10.1073/pnas.1522469113>.
48. Collins CR, Hackett F, Strath M, Penzo M, Withers-Martinez C, Baker DA, Blackman MJ. 2013. Malaria parasite cGMP-dependent protein kinase regulates blood stage merozoite secretory organelle discharge and egress. *PLoS Pathog* 9:e1003344. <https://doi.org/10.1371/journal.ppat.1003344>.
49. Thomas JA, Collins CR, Das S, Hackett F, Graindorge A, Bell D, Deu E, Blackman MJ. 2016. Development and application of a simple plaque assay for the human malaria parasite *Plasmodium falciparum*. *PLoS One* 11:e0157873. <https://doi.org/10.1371/journal.pone.0157873>.
50. MacPherson CR, Scherf A. 2015. Flexible guide-RNA design for CRISPR applications using Protospacer Workbench. *Nat Biotechnol* 33:805–806. <https://doi.org/10.1038/nbt.3291>.
51. Mohring F, Hart MN, Patel A, Baker DA, Moon RW. 2020. CRISPR-Cas9 genome editing of *Plasmodium knowlesi*. *Bio Protoc* 10:e3522. <https://doi.org/10.21769/BioProtoc.3522>.
52. Bennett TN, Paguio M, Gligorijevic B, Seudieu C, Kosar AD, Davidson E, Roepe PD. 2004. Novel, rapid, and inexpensive cell-based quantification of antimalarial drug efficacy. *Antimicrob Agents Chemother* 48:1807–1810. <https://doi.org/10.1128/AAC.48.5.1807-1810.2004>.
53. Smilkstein M, Sriwilaijaroen N, Kelly JX, Wilairat P, Riscoe M. 2004. Simple and inexpensive fluorescence-based technique for high-throughput antimalarial drug screening. *Antimicrob Agents Chemother* 48:1803–1806. <https://doi.org/10.1128/AAC.48.5.1803-1806.2004>.
54. Diarra A, Sheldon C, Church J. 2001. In situ calibration and [H<sup>+</sup>] sensitivity of the fluorescent Na<sup>+</sup> indicator SBFI. *Am J Physiol Cell Physiol* 280:C1623–C1633. <https://doi.org/10.1152/ajpcell.2001.280.6.C1623>.
55. Harootunian AT, Kao JP, Eckert BK, Tsien RY. 1989. Fluorescence ratio imaging of cytosolic free Na<sup>+</sup> in individual fibroblasts and lymphocytes. *J Biol Chem* 264:19458–19467. [https://doi.org/10.1016/S0021-9258\(19\)47322-5](https://doi.org/10.1016/S0021-9258(19)47322-5).
56. Yang J, Yan R, Roy A, Xu D, Poisson J, Zhang Y. 2015. The I-TASSER Suite: protein structure and function prediction. *Nat Methods* 12:7–8. <https://doi.org/10.1038/nmeth.3213>.
57. Trott O, Olson AJ. 2010. AutoDock Vina: improving the speed and accuracy of docking with a new scoring function, efficient optimization, and multithreading. *J Comput Chem* 31:455–461. <https://doi.org/10.1002/jcc.21334>.
58. Pettersen EF, Goddard TD, Huang CC, Couch GS, Greenblatt DM, Meng EC, Ferrin TE. 2004. UCSF Chimera—a visualization system for exploratory research and analysis. *J Comput Chem* 25:1605–1612. <https://doi.org/10.1002/jcc.20084>.